Applied Thermal Engineering 195 (2021) 117237

Contents lists available at ScienceDirect

Applied Thermal Engineering

journal homepage: www.elsevier.com/locate/apthermeng

Heat transfer analysis of rectangular porous fins in local thermal non-equilibrium model

Bernardo Buonomo [a,*], Furio Cascetta [a], Oronzio Manca [a], Mikhail Sheremet [b]

[a] Dipartimento di Ingegneria, Università degli Studi della Campania "Luigi Vanvitelli", Via Roma 29, Aversa, Italy
[b] Laboratory on Convective Heat and Mass Transfer, Tomsk State University, Tomsk, Russia

ARTICLE INFO

Keywords:
Porous fin
Local thermal non-equilibrium
Natural convection
Radiation
Adomian decomposition Method
Local thermal equilibrium assumption criteria

ABSTRACT

In this study, an analytical solution of a porous fin with natural convection and radiation heat transfer is carried out. For the first time, the analysis is accomplished in Local Thermal Non-Equilibrium (LTNE) model. The investigation is carried out on a porous fin with finite length and adiabatic tip. The Darcy model and Boussinesq approximation for buoyancy effects are used to evaluate the infiltration velocity in the porous medium. Two energy equations are solved using the Adomian Decomposition Method (ADM). The solution is validated with the numerical solution of the finite difference method, and with the asymptotic solution for the Local Thermal Equilibrium (LTE) model. The results are presented in terms of temperature profiles and total average Nusselt numbers. They pointed out the effects of internal and external radiation and convection heat transfer, as well as thermal conductivity ratio and dimensionless thickness. It was found that solid phase temperature profiles decrease as the Biot, *Bi*, and Rayleigh, *Ra**, numbers decrease, whereas the difference between the solid phase and fluid phase temperatures, for assigned *Bi*, decreases for lower *Ra*. Thermal conductivity ratio and dimensionless thickness increase engender higher solid phase temperature for assigned *Bi* and *Ra**. The total Nusselt number increases as *Ra**, *Bi* and external radiation increase, whereas it decreases with the thermal conductivity ratio. Criteria to compare LTNE and LTE assumptions are proposed, and they highlight the fact that the minimum Biot number to accept the LTE assumption becomes lower as the Rayleigh number decreases.

1. Introduction

Nowadays, growing need for the miniaturization of devices in a wide range of applications has engendered strong interest in heat transfer research, for the realization of optimal thermal performance, in very small volume(s). This means that heat transfer rate per unit of volume increases significantly, which allows for the realization of more compact components in a variety of engineering applications, such as heat exchangers, thermal energy storages, thermal control in electronic components, solar collectors, and so on. Some efficient techniques to enhance heat transfer, are related to the use of extended surfaces [1,2] and porous media [2,3]. Porous fins combine advantages of two techniques, thereby increasing the ratio between the heat transfer area and the volume, which are employed in several applications [4–9]. In the last decade, research activities on porous fins have increased significantly, as shown in a review paper [9].

One of the first pioneering works on porous fin in single phase was accomplished by Kiwan and Al-Nimr [10]. The analysis was accomplished by solving the coupled problem between the porous or solid fins and fluid, by means of a finite element technique. The porous medium was treated adopting the Brinkman-Forchheimer-extended Darcy model in local thermal equilibrium (LTE) assumption. The results show a significant advantage in the use of porous fin, compared with solid fin, in terms of performance, particularly increasing the Rayleigh number at high Darcy numbers. A simple model of single rectangular porous fin in natural convection was studied by Kiwan [11] employing Darcy's model in LTE assumption. The comparison with the complete model proposed in [10] shows that the evaluation of the heat transfer rates by the simple model, was within an accuracy of 10%. The extension of the model in [11] to the effect of radiative heat transfer and the external convective heat transfer in a rectangular porous fin, was given by Kiwan [12]. Khaled [13] investigated rectangular porous fin with surface heat losses, through a convective heat transfer, and an internal heat transfer due to the flow through the permeable fin. The analysis was accomplished in LTE assumption. The enhancement of forced convection in an

* Corresponding author at: Dipartimento di Ingegneria, Università degli Studi della Campania "Luigi Vanvitelli", Via Roma, 29, 81031 Aversa, CE, Italy.
E-mail addresses: bernardo.buonomo@unicampania.it (B. Buonomo), furio.cascetta@unicampania.it (F. Cascetta), oronzio.manca@unicampania.it (O. Manca), michael-sher@yandex.ru (M. Sheremet).

https://doi.org/10.1016/j.applthermaleng.2021.117237
Received 9 January 2021; Received in revised form 12 May 2021; Accepted 9 June 2021
Available online 16 June 2021

Nomenclature

a_{sf}	interfacial area per unit of volume of porous fin, m^{-1}
$A_b = Wt$	cross-section area of the fin, m^2
A_n	Adomian polynomial
A_{sf}	interfacial area between fluid and solid phases, m^2
Bi	Biot number, eq. (16)
c_{pf}	specific heat of fluid, J kg^{-1} K^{-1}
Err	defined in Eq. (44)
g	acceleration of gravity, m s^{-2}
h_L,	external convective heat transfer coefficient, W m^{-2} K^{-1}
h_{sf}	convective heat transfer coefficient between solid and fluid phases in porous fin, W m^{-2} K^{-1}
k	thermal conductivity, W m^{-1} K^{-1}
K	permeability of porous fin, m^2
L	length of porous fin, m
L_X	differential operator
$\dot{m}$	mass flow rate, kg s^{-1}
Nu	Nusselt number
P	cross section perimeter, m
q	heat transfer flux, W m^{-2}
q_x	conductive heat transfer flux component, along $\times$, W m^{-2}
$\dot{Q}$	heat transfer rate
R_1	surface-ambient radiation parameter, eq. (16)
Ra^*	Rayleigh number for porous medium, eq. (16)
R_d	radiation–conduction parameter, eq. (16)
t	thickness of porous fin, m
T_∞	ambient temperature, K
T_b	temperature of the porous fin base, K
T	temperature, K
x	axial coordinate, m
X	dimensionless axial coordinate
v_w	velocity in the porous fin, m s^{-1}
W	width of the porous fin, m

Greek symbols

β	coefficient of volumetric expansion, K^{-1}
β_R	Rosseland mean extinction coefficient, m
ν	kinematic viscosity, m^2 s^{-1}
φ	porosity
ε	emissivity coefficient
θ	dimensionless temperature, eq. (16)
χ	dimensionless parameter, eq. (16)
κ	thermal conduction ratio, eq. (16)
τ	dimensionless thickness, eq. (16)
λ	external convective heat transfer coefficient, eq. (16)
σ	Stefan-Boltzmann constant, W m^{-2} K^{-4}
ρ	density, kg m^{-3}

Subscripts

b	base of fin
f	fluid
eq	effective
l	local scale length
L	system length scale, i.e., porous fin length
s	solid
s,f	solid–fluid interface
t	total

isothermal parallel-plate duct by porous fins attached to both plates, was investigated numerically by Hamdan and Al-Nimr [14]. The analysis inside the porous medium was provided considering the Darcy–-Brinkman–Forchheimer model and in LTE assumption. The results show that heat transfer was enhanced while employing high conductive porous fins, low Darcy number values and by increasing microscopic inertial coefficient.

An analysis of three different cases of rectangular porous fin was accomplished by Gorla and Bakier [15]. The Darcy model in LTE hypothesis was used to describe the porous medium while considering the contribution of radiative heat transfer. The results pointed out that radiative heat transfer gives a significant contribution with respect to a similar case without radiation. Three models to analyze the heat transfer from a rectangular porous fin, with and without radiation, were studied by Kundu and Bhanja [16]. The analysis was performed in Darcy model with the LTE assumption and solving the nonlinear governing equation with a decomposition method. The effects of the thermal and geometrical variables on temperature distribution, fin performance and its optimum dimensions were evaluated. The evaluation of temperature profiles and performance parameter of a T-shaped porous fin was provided by Bhanja and Kundu [17]. The governing equation was written applying the Darcy model and in LTE assumption, taking into account, natural convection and radiation. The solutions for different geometrical and thermal parameter values were found by a decomposition technique. The dependence on different parameters was investigated and the results highlighted the increase in heat transfer, related to the porosity. A heat transfer analysis on rectangular porous fin in natural convection was accomplished by Rahimi Petroudi et al [18]. The nonlinear governing equation in Darcy and LTE hypothesis was solved by means of the homotopy perturbation method (HPM). Kundu et al. [19] provided an analysis on the performance and optimal design of straight porous fins with different profiles. The Adomian decomposition technique was used to solve the nonlinear governing equation for natural convection in Darcy model and LTE assumption. The results indicate that the porous fins presented a considerable heat transfer enhancement with respect to the solid fins, when the porosity and flow parameter assume low and high values, respectively.

An investigation on rectangular porous fin with effect of convective and radiative heat transfer was given by Torabi and Yaghoobi [20]. The method of differential transformation was used to find the solution of the nonlinear governing equation, which was written considering the Darcy model and LTE assumption for the porous medium. A comparison with the numerical solution by a fourth-order Runge-Kutta technique was accomplished. The results were similar to the previous studies. The same problem was studied by Dravishi et al. [21] employing the homotopy analysis method (HAM). Solutions were derived for the classical three cases of fin problem. Saedodin and Shahbabaei [22] evaluated the temperature distribution in a rectangular porous fin subjected to natural convection by a homotopy perturbation method. The nonlinear governing equation considered the Darcy model and LTE assumption.

A porous pin fin under natural convection heat transfer was studied by Bhanja et al. [23] employing the Darcy model and the LTE assumption. The solution was carried out using Adomian decomposition method and a comparison with a numerical solution, evaluated by means of the finite difference method, was performed. The convenience to use the porous pin fin was noted for some porous medium conditions. The porous pin fin in natural convection was also investigated by Saedodin and Sadeghi [24] employing the Darcy model and LTE assumption. The solution was found for the case with infinite length by means of the Runge-Kutta fourth-order method. The impacts of porosity and convection parameters were investigated and compared with solid fin.

A rectangular porous fin under a natural convection condition and with temperature dependent internal heat generation was analyzed by Hatami et al. [25]. Solutions for the nonlinear governing equation in Darcy model and LTE assumption were carried out by collocation

method, differential transformation method, and least square method, and compared to the numerical solution obtained by a fourth–fifth order Runge–Kutta–Fehlberg procedure. An analysis of circular porous fins subjected to natural convection and radiation heat transfer was provided by Hatami and Ganji [26]. The governing equations for four different profiles were defined considering the Darcy model and the LTE assumption and solved by least square method and fourth order Runge–Kutta method. One of the main results was that exponential profile presented the largest heat transfer rate.

A rectangular moving porous fin with radiation and natural convection heat transfer was studied by Moradi et al. [27]. The analysis was accomplished under the hypothesis of Darcy model and LTE approach. The nonlinear governing equation was solved using homotopy analysis method. The solutions were evaluated for finite length with adiabatic tip and infinite length fins.

The analysis of a porous triangular fin under radiation and natural convection heat transfer conditions with temperature dependent thermal conductivity, was accomplished by Moradi et al. [28]. The governing equation for Darcy model and LTE assumption was solved by differential transformation method and compared with the results given by fourth order Runge–Kutta method. The results stressed that the use of porous medium improved fin performance. The extension to the moist air stream of the study on circular porous fins given in [26] was presented by the same authors, Hatami and Ganji, in [29]. The heat transfer was related to natural convection only and the porous medium was modeled with Darcy law and under LTE assumption. The nonlinear governing equation was solved considering least square method and fourth order Runge-Kutta method. Straight porous fins with different profiles were investigated considering the radiative and convective heat transfer by Hatami and Ganji [30]. The nonlinear governing equations with Darcy model and LTE assumption were solved by means of fourth order Runge–Kutta method and least square method. An interesting result was that the exponential profile for Si_3N_4 material presented the highest heat transfer rate. Different profiles of straight porous fin were studied by Turkyilmazoglu [31] with the heat and mass transfer simultaneously. Analytical solutions for all profiles were found employing the Darcy model and the LTE hypothesis together with constant convective coefficients.

An investigation on cylindrical porous fins with radiative and convective heat transfer was numerically performed by Das [32]. The solution of governing equation given under Darcy and LTE hypothesis was carried out by Runge–Kutta method. Moreover, an inverse technique was used to estimate the unknown parameters. Radiation and convection heat transfer from a straight porous fin was studied by Kundu and Lee [33] to evaluate its minimum shape. The governing equation was assumed for Darcy model, LTE model and temperature dependent surface heat transfer coefficient. The analysis was performed by means of the variational calculus. A straight porous fin problem with convective heat transfer, using the Darcy model, was studied by Shahbabaei and Ganji [34]. The nonlinear equation for LTE assumption was solved by a collocation method. A study of porous pin fins with different longitudinal profiles was analyzed by Vahabzadeh et al. [35] for moist air and Darcy model. The nonlinear governing equations in LTE assumption and temperature dependent convective heat transfer were solved by the least square method. A porous radial fin with convection and radiation heat transfer was studied by Darvishi et al. [36]. The porous medium was considered in Darcy model and the nonlinear governing equation in LTE assumption was solved by a series developed with homotopy analysis method. A validation of the results was provided with the comparison with a numerical method. The nonlinear equation related to rectangular porous fins with convective heat transfer, Darcy model and LTE assumption was solved by Cuce and Cuce [37] using the homotopy perturbation method. An excellent agreement with the results carried out by finite difference method was observed. An analysis on rectangular porous fins employing Adomian decomposition Sumudu transform method was provided by Deshamukhya and Meher [38]. The governing equation was written considering the Darcy model and LTE assumption. The results were in sync with the ones carried out by means of the homotopy perturbation method.

A rectangular porous fin with radiation and natural convection heat transfer for moist air was investigated by Darvishi et al. [39]. The Darcy model and LTE assumption were considered to examine the governing equation and the spectral collocation method was applied to find the solution. An annular moving fin with radiative-convective heat transfer and volumetric heat generation was analyzed by Kundu and Lee [40]. The nonlinear governing equation was written for Darcy model, LTE assumption and a linear temperature dependent heat generation. The solution was carried out by the double differential transform method. The Adomian decomposing technique to evaluate the thermal behavior of a rectangular porous stepped fin was accomplished by Singh et al. [41] with radiation and natural convection heat transfer. The temperature dependent heat generation inside the fin was taken into account and the Darcy model and LTE assumption in the nonlinear energy equation were considered. An analysis of rectangular porous fins with radiation and convection heat transfer was performed by Ma et al. [42]. The governing equations for temperature dependent internal heat generation and surface convection were written, considering the Darcy model and LTE assumption. A spectral collocation method was used to evaluate the temperature distribution. A radial porous fin with moist air, radiation and convection heat transfer was investigated by Khani et al. [43]. The nonlinear governing equation was formulated using the Darcy model and LTE assumption. The spectral collocation method was developed employing the Chebyshev polynomials. An investigation on radial porous fins with convective and radiative heat transfer was provided by Motsumi [44] for temperature dependent thermal conductivity. In the energy equation, the Darcy model and LTE assumption were considered, and the nonlinear problem was numerically solved by shooting technique and Runge-Kutta-Fehlberg method.

A study of a T-shaped porous fin with convective mass and heat transfer was proposed by Hazarika et al. [45]. The analysis was accomplished with Darcy model and LTE assumption, and the corresponding nonlinear governing equations were solved, employing the differential transform method.

Straight moving porous fins with different longitudinal profiles were studied by Ma et al. [46]. The governing equation for porous fins in radiative and convective heat transfer was considered assuming the Darcy and LTE hypothesis. A spectral technique employing Chebyshev polynomials was used to carry out the solutions for the cases with heat generation. A thermal analysis of a rectangular porous fin with natural convection and temperature dependent heat generation was accomplished by Asadian et al. [47]. The nonlinear energy equation was written using the Darcy model and the LTE assumption. It was resolved employing Galerkin's and Akbari-Ganji's methods. A similar problem given in [47] was solved by Sobamowo et al. [48] by means of the Galerkin's method of weighted residual. Temperature distributions in a rectangular porous fin with adiabatic and convective conditions on the tip were evaluated by Deshamukhya et al. [49]. The governing equation given in Darcy model and LTE assumption was solved by Adomian decomposition method. An extension of work given in [47] to straight porous fins with different longitudinal profiles was provided by Shateri and Salahshour [50]. They solved the nonlinear energy equation by the least square method. A rectangular porous fin with radiative and natural convection heat transfer was analytically and numerically examined by Hoshyar et al. [51]. The energy equation with temperature dependent convective coefficient, emissivity and internal heat generation was formulated in Darcy model and LTE assumption. Solutions were evaluated by least square, homotopy analysis and collocation methods and a comparison with the numerical analysis carried out by fourth-order Runge–Kutta method was performed. A circular porous fin with constant thickness under radiative and convective heat transfer was studied by Zagar et al. [52]. The governing equation with temperature dependent heat generation, convective coefficient and thermal conductivity,

was written assuming the Darcy model and LTE. The homotopy analysis method was used to evaluate the solution. A convective rectangular porous fin, with temperature dependent internal heat generation, was investigated by Hoseinzadeh et al. [53]. The nonlinear governing equation in Darcy and LTE assumptions was solved by collocation method, homotopy perturbation and analysis methods.

A rectangular inclined porous fin with natural convection and a constant heat flux was analyzed by Kiwan [54]. The governing equation was considered under Darcy model and LTE, and the solution for the base temperature was given in closed form.

A thermal analysis of radiative-convective rectangular porous fins with linear temperature dependent heat generation was performed by Hoseinzadeh et al. [55]. The homotopy analysis method was applied to solve the nonlinear energy equation considered in Darcy and LTE hypothesis. An investigation on rectangular porous fins, with natural convection, was presented by Abbasbandy and Shivanian [56]. The energy equation with temperature dependent thermal conductivity and internal generation was considered under Darcy model and LTE assumption.

A radial porous fin in moist air with radiation and natural convection was numerically studied by Gireesha et al. [57]. The nonlinear governing equation written under Darcy and LTE hypothesis, was solved by means of the finite element method. A straight moving porous fin with rectangular and exponential longitudinal profiles was investigated with radiative and natural convective heat transfer by Ndlovu and Moitsheki [58]. The nonlinear energy equation was formulated with Darcy and LTE assumptions and solved by the differential transform technique. Circular porous fins with rectangular, triangular and convex profiles with natural convection heat transfer were studied by Shafiei and Talaghat [59] considering a temperature dependent surface heat transfer. The nonlinear energy equation was developed considering the Darcy model and LTE assumption and the solutions were carried out by means of the Galerkin method and a finite difference method.

A study of moving rectangular porous fins with radiative and convective heat transfer was performed by Ndlovu and Moitsheki [60]. The nonlinear governing equation, written in Darcy model and LTE assumption, was solved by the variational iteration method. A rectangular porous fin with radiation and convection heat transfer was analyzed in moist air by Sowmya et al. [61]. The solution of nonlinear energy equation under Darcy model and LTE assumption was carried out by means of Runge–Kutta–Fehlberg fourth–fifth-order method. An analysis of thermal parameters of straight porous fins of different longitudinal profiles between two plates, at assigned temperature, was provided by Gupta et al. [62]. The governing equation was formulated considering natural convection, Darcy model and LTE assumption. A finite difference method with an iterative solver and weighted residual Galerkin method, were used to evaluate the solutions. A rectangular porous fin in moist air with radiation and convection heat transfer was studied by Sowmya et al. [63] considering three different functions of temperature dependent thermal conductivity. The nonlinear energy equation in Darcy and LTE formulation was solved by means of Runge-Kutta-Fehlberg fourth-fifth order method. The thermal analysis for an inclined rectangular porous fin given in [54] was extended by Gireesha and Sowmya [64] to the case with radiative heat transfer. The nonlinear energy equation considered in Darcy and LTE assumptions was solved by means of a differential transform method. A comparison with the results obtained by Adomian decomposition and Runge–Kutta–Fehlberg techniques was accomplished.

The reviewed contributions on porous fins with gas or moist air are summarized in Table 1, where the geometry of the porous fin, the effect considered as convective, radiative and mass transfer as moist air, and the solution method are reported. Suffice it to say that many other contributions related to the porous fins are available in open literature. They are on inverse problem [20,65,66], experimental investigations [4,5,8,67], porous fins interacting with nanofluids [68–72], optimization problems [16,73–79], porous fin with magnetic fields [80–85] and transient analysis [83,86-88]. More so, several engineering applications are related to porous fins, such as heat exchangers [75,89-94], solar still and photovoltaic systems [4,5,95], closed cavities in natural convection [96-98], and heat sink in electronic cooling [6,7,77,99–101].

As a matter of fact, it is noteworthy that in all investigations on porous fins, as reported in Table 1, only the local thermal equilibrium (LTE) model has been assumed. The derived mathematical problem, for the porous fins in different physical phenomena, is related to nonlinear ordinary differential equations (ODE) problem. Several approaches to evaluate the solutions have been used, as indicated in Table 1. However, as underlined by several researchers [102-112], for the porous media where solid and fluid phases present significant differences among their local temperatures, the local thermal non-equilibrium (LTNE) model is more appropriate to describe a porous fin. Minkowycz et al. [106] provided the conditions to employ the LTE model in terms of Sparrow number ($Sp > 100$). Moreover, it should be underlined that many solutions related to different problems in porous media for local thermal non equilibrium (LTNE) conditions are collected in [2,3,106,112]. Despite the countless solutions related to porous media treated in LTNE model, to the authors' best knowledge, the LTNE model seems not to be considered in heat transfer analysis in porous fins.

In the present study, an investigation on rectangular porous fin with natural convection and radiation heat transfer, adopting the LTNE model, has been developed for the first time. The investigation presents a new solution for rectangular porous fin with the assumption of LTNE which represents an innovative approach to the porous fin problems in general. The analysis is carried out for a porous fin with finite length and adiabatic tip in Darcy model and the solution of the energy equations is carried out by using the Adomian Decomposition Method (ADM). Results to show the effect of different relevant parameters on solid and fluid dimensionless temperature profiles and total Nusselt number are presented. The study allows to evaluate the solid and fluid temperature profiles inside a rectangular porous fin with adiabatic tip, as well as the dimensionless heat transfer coefficient, from the porous fin. Moreover, criteria to use the LTE or the LTNE assumptions are given.

2. Governing equations and mathematical model

The analyzed physical problem is on rectangular porous fin attached to a vertical wall with natural convection and radiation heat transfer, as shown in Fig. 1. The cross-section area of the fin, $A_b = Wxt$, is assumed constant along the longitudinal axis $\times$, where W and t are width and thickness of the porous fin, respectively. The length of the fin is L. Since the fin is porous, the buoyancy force induced by constant temperature of the base surface, where the porous fin is placed, T_b, involves the passage of fluid through it.

The analysis is conducted considering the following assumptions:

- the porous material is homogeneous, isotropic and saturated with a single-phase fluid;
- all the thermo-physical properties of the fluid and the solid matrix of the porous medium are temperature independent except for the density in the buoyancy term (Boussinesq approximation);
- the temperature inside the porous fin is only a function of the longitudinal coordinate $\times$ along the length L of the fin, and the heat conduction is along the $\times$ axis;
- the Darcy model is applied to describe the momentum interaction between the porous fin and the fluid. The motion of the fluid due to the buoyancy effect is orthogonal to the length L of the fin;
- natural convection on the outer surface of the fin is in place;
- radiative effects in the porous fin and between the outer surface of the fin and the surrounding environment are taken into account, and a constant emissivity is assumed;
- thermal contact resistances at the fin base and heat sources inside the fin all have zero value;

Table 1
Studies on porous fins.

Reference	Geometry	Effect considered	LTE LTNE	Analytical or Numerical Method
Kiwan&Al-Nimr (2001) [10]	straight fins with rectangular profile	Mixed convection	LTE	Finite Element Method by FIDAP
Kiwan. (2007) [11]	straight fins with rectangular profile	Natural convection	LTE	Fourth order Runge–Kutta method
Kiwan (2007) [12]	straight fins of rectangular profile	Natural convection and radiation	LTE	Analytical solution and finite difference method
Khaled (2010) [13]	rectangular porous fins	Forced convection	LTE	Finite difference equation
Hamdan et al. (2010) [14]	porous fins between the two parallel plates.	Forced convection	LTE	Finite difference method
Gorla and Bakier (2011) [15]	Rectangular profile fin	Natural convection and radiation	LTE	Fourth order Runge–Kutta method
Kundu and Bhanja (2011) [16]	straight fins of rectangular profile	Natural convection and radiation	LTE	Adomian decomposition method
Bhanja and Kundu (2011) [17]	Constructal T-shape porous fin	Natural convection and radiation	LTE	Adomian decomposition method
Rahimi Petroudi et al. (2012) [18]	rectangular fin profile	natural convection	LTE	homotopy perturbation method
Kundu et al. (2012) [19]	straight fins of rectangular, convex parabolic and two exponential profiles	Natural convection	LTE	Adomian decomposition method
Torabi and Yaghoobi (2013) [20]	rectangular stepped fin profile	natural convection and radiation effect	LTE	Differential transformation method
Darvishi et al. (2013) [21]	straight fins with rectangular profile	Natural convection and radiation	LTE	Homotopy analysis method (HAM)
Saedodin and Shahbabaei (2013) [22]	straight fins with rectangular profile	Natural convection	LTE	Homotopy perturbation method (HPM)
Bhanja et al. (2013) [23]	straight fins with circular section.	Natural convection	LTE	Adomian decomposition method
Saedodin and Sadeghi (2013) [24]	cylindrical fin profile	natural convection	LTE	Runge–Kutta fourth-order method
Hatami et al. (2013) [25]	straight fins	Generation and natural convection	LTE	Least Square Method (LSM) and fourth order Runge–Kutta method
Hatami and Ganji (2013) [26]	circular fins of rectangular convex, triangular and exponential profiles	natural convection and radiation	LTE	Least Square Method (LSM) and fourth order Runge–Kutta method
Moradi et al. (2014) [27]	straight moving fins with rectangular profile	Natural convection and radiation heat transfer	LTE	Homotopy analysis method (HAM)
Moradi et al. (2014) [28]	Triangular fins	Natural convection and radiation, temperature-dependent thermal conductivity	LTE	Differential transformation method (DTM)
Hatami and Ganji (2014) [29]	circular fins of rectangular convex and triangular profiles	Natural convection in air stream.	LTE	Least Square Method (LSM)and fourth order Runge-Kutta method
Hatami and Ganji (2014) [30]	straight fins of rectangular convex, triangular and exponential profiles	generation, natural convection and radiation	LTE	Least Square Method (LSM) and fourth order Runge–Kutta method
Turkyilmazoglu (2014) [31]	Various fin profiles	Convection	LTE	Analytic solution
Das (2014) [32]	Cylindrical porous fin	Natural convection and radiation	LTE	Runge–Kutta method
Kundu and Lee (2015) [33]	Optimum shape of fins	Natural convection and radiation, temperature-dependent heat transfer coefficient	LTE	Adomian decomposition method
Shahbabaei and Ganji (2015) [34]	straight finwith variable cross section	Natural convection	LTE	Collocation Method (CM) and comparison with HAM, VIM, BVP*
Vahabzadeh et al. (2015) [35]	Pin fins with variable cross section	Forced convection, moist air	LTE	Least Square Method (LSM) and fourth order Runge–Kutta method
Darvishi et al. (2015) [36]	Radial (circular) fin of rectangular profile	Natural convection and radiation	LTE	Homotopy analysis method (HAM)
Cuce and Cuce (2015) [37]	straight fins	Natural convection	LTE	Homotopy perturbation method (HPM)
Patel and Meher (2015) [38]	longitudinal porous fins	Natural convection	LTE	Adomian decomposition Sumudu transform method (ADSTM)
Darvishi et al. (2016) [39]	straight fin	natural convection and radiation, moist air	LTE	Spectral collocation method
Kundu and Lee (2016) [40]	annular step porous moving fins	Natural convection and radiation heat transfer	LTE	Differential Transformation Method (DTM)
Singh et al.(2016) [41]	porous stepped fin	Natural convection and radiation	LTE	Adomian decomposition method
Ma et al (2016) [42]	straight fins with rectangular profile	convective–radiative and temperature dependent internal heat generation	LTE	Spectral collocation method (SCM)
Khani et al (2016) [43]	radial fin	natural convection and radiation effect	LTE	Spectral collocation method
Motsumi (2016) [44]	radial fins	convective and radiative heat transfer	LTE	Shooting technique and Runge-Kutta-Fehlberg method
Hazarika et al. (2017) [45]	T-shaped porous fin	convective mass and heat transfer	LTE	differential transform method
Ma et al. (2017) [46]	moving porous fins of trapezoidal, convex parabolic and concave parabolic profiles	Natural convection, radiation heat transfer and heat generation	LTE	Spectral element method (SEM)
Asadian et al. (2017) [47]	rectangular porous fins	natural convection and temperature dependent heat generation	LTE	Galerkin's method and Akbari-Ganji's method

(*continued on next page*)

Table 1 (*continued*)

Reference	Geometry	Effect considered	LTE LTNE	Analytical or Numerical Method
Sobamowo et al. (2017) [48]	straight porous fin	Natural convection, radiation heat transfer and heat generation	LTE	Galerkin's method of weighted residual
Deshamukhya et al. (2017) [49]	rectangular porous fin	natural convection	LTE	Adomian decomposition method
Shateri and Salahshour (2018) [50]	rectangular, trapezoidal, and concave cross-sectional areas	Natural convection, radiation heat transfer and heat generation	LTE	Least squares method (LSM) and finite difference technique
Hoshyar et al (2019) [51]	rectangular porous fin	Natural convection, radiation heat transfer and heat generation	LTE	collocation method, the least square method and homotopy analysis method
Zargar et al (2019) [52]	circular porous fin	convective-radiative and internal heat generation	LTE	homotopy analysis method
Hoseinzadeh et al. (2019) [53]	rectangular porous fin	convective and internal heat generation	LTE	collecation method, homotopy perturbation and analysis methods
Kiwan (2019) [54]	rectangular inclined porous fin	natural convection and constant heat flux	LTE	solution for base temperature in closed form
Hoseinzadeh et al. (2019) [55]	rectangular porous fin	convective-radiative and internal heat generation	LTE	homotopy analysis method
Abbasbandy and Shivanian (2019) [56]	rectangular porous fin	natural convection and internal heat generation	LTE	exact analytical solution in implicit form
Gireesha et al. (2019) [57]	moving radial porous fin	moist air with radiation and natural convection	LTE	finite element method
Ndlovu and Moitsheki (2019) [58]	moving straight porous fin with rectangular and exponential longitudinal profiles	radiative and natural convective heat transfer	LTE	differential transform method
Shafiei and Talaghat (2019) [59]	Circular porous fin with rectangular, triangular and convex profiles	natural convection	LTE	finite difference method and Galerkin's method
Ndlovu and Moitsheki (2020) [60]	moving rectangular porous fin	radiative and convective heat transfer	LTE	variational iteration method
Sowmya et al. (2020) [61]	variational iteration method	radiation and convection heat transfer, moist air	LTE	Runge–Kutta–Fehlberg fourth–fifth-order method
Gupta et al. (2020) [62]	straight porous fins of different longitudinal profiles	natural convection	LTE	finite difference method with iterative solver and weighted residual Galerkin method
Sowmya et al. (2020) [63]	rectangular porous fin	in moist air with radiation and convection heat transfer	LTE	Runge-Kutta-Fehlberg fourth-fifth order method
Gireesha and Sowmya (2020) [64]	rectangular inclined porous fin	radiation and convection heat transfer	LTE	Differential Transform Method

Local thermal equilibrium (LTE), Local thermal non equilibrium (LTNE).

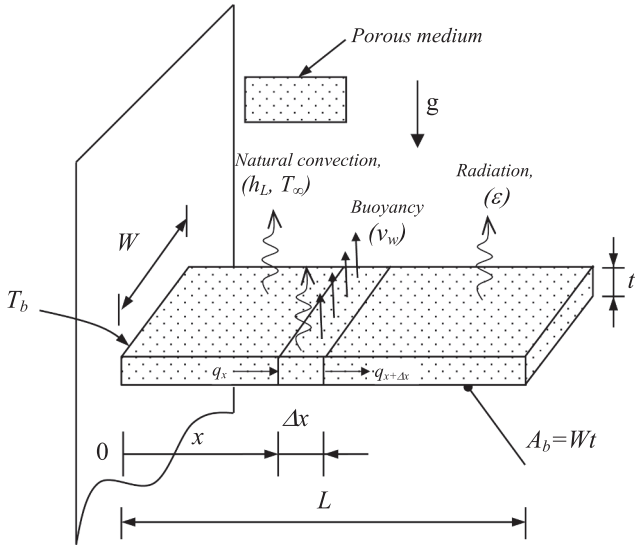

Fig. 1. Geometry sketch of the porous fin.

- the hypothesis of local thermal non-equilibrium (LTNE) is considered to model the thermal interaction between fluid and porous fin. With this assumption the fluid and solid temperatures are locally different.
- the surface porosity and the volumetric porosity are equal.

Under these hypotheses the energy equations for fluid and solid phases at steady state, are:

fluid phase

$$\dot{m}c_{pf}\left(T_f - T_\infty\right) = h_{sf}A_{s,f}\left(T_s - T_f\right) + A_b q_f(x) - A_b q_f(x+dx) \tag{1}$$

solid phase

$$A_b\dot{q}_s(x) - A_b\dot{q}_s(x+\Delta x) = h_L P\Delta x(1-\varphi)(T_s - T_\infty) + P\Delta x\sigma\varepsilon\left(T_s^4 - T_\infty^4\right) + h_{sf}A_{sf}\left(T_s - T_f\right) \tag{2}$$

where T_f, T_s and T_∞, are the temperature of the fluid phase, solid phase and of the ambient respectively;φ is the porosity; ε is emissivity coefficient and σ is Stefan-Boltzmann constant; h_{sf} and A_{sf} are the convective heat transfer coefficient and the interfacial area between fluid and solid phases inside the porous fin, respectively; h_L is external convective heat transfer coefficient.

The left-hand side of Eq. (1) represents the amount of energy transferred to the fluid crossing the porous medium. The infiltration of the fluid in the porous medium is due to the buoyancy force induced by the temperature difference between the base of the fin and the surrounding environment. The first term on the right-hand side of Eqs. (1) and (2) represents the convective heat exchange between fluid and solid phases. The term is due to the local thermal non-equilibrium (LTNE) assumption. The last two terms on the right-hand side of Eq. (1) represent the net heat transfer rate from the base to the fin element by conduction. The effect of radiation heat transfer appears in two terms in Eq. (2); the left-hand side, which represents the net heat transfer rate from the base to element by conduction and radiation, and the second term on the right-hand side of Eq. (2) which denotes the radiative heat transfer rate between the surfaces of the fin and surrounding ambient. Finally, the first term on the right-hand side of Eq. (2) corresponds to convective heat transfer through the fin surface.

The mass flow rate of the fluid induced by the buoyancy force can be written as [11]:

$$\dot{m} = \rho_f (W \cdot \Delta x) v_w \tag{3}$$

where v_w is the velocity of the fluid passing through the porous material due to the buoyancy. By invoking the Darcy model, the infiltration velocity v_w can be evaluated as [2,3,11]:

$$v_w = \frac{gK\beta}{\nu}\left(T_f - T_\infty\right) \tag{4}$$

Substituting Eqs. (3) and (4) for Eqs. (1) and (2), and dividing by term $A_b \cdot \Delta x$, the following obtains:

$$\frac{\dot{q}_f(x) - \dot{q}_f(x+\Delta x)}{\Delta x} = \frac{h_{sf} A_{s,f}}{A_b \Delta x}\left(T_f - T_s\right) + \frac{\rho_f c_{pf} g K \beta}{\nu t}\left(T_f - T_\infty\right)^2 \tag{5}$$

$$\frac{\dot{q}_s(x) - \dot{q}_s(x+\Delta x)}{\Delta x} = \frac{h_L P(1-\varphi)}{A_b}\left(T_s - T_\infty\right) + \frac{P\sigma\varepsilon}{A_b}\left(T_s^4 - T_\infty^4\right) + \frac{h_{sf} A_{sf}}{A_b \Delta x}\left(T_s - T_f\right) \tag{6}$$

For, $\Delta x \to 0$, Eqs. (5) and (6) become:

$$-\frac{d\dot{q}_f(x)}{dx} = \frac{h_{sf} a_{s,f}}{A_b}\left(T_f - T_s\right) + \frac{\rho_f c_{pf} g K \beta}{\nu t}\left(T_f - T_\infty\right)^2 \tag{7}$$

$$-\frac{d\dot{q}_s(x)}{dx} = \frac{h_L P(1-\varphi)}{A_b}\left(T_s - T_\infty\right) + \frac{P\sigma\varepsilon}{A_b}\left(T_s^4 - T_\infty^4\right) + \frac{h_{sf} a_{sf}}{A_b}\left(T_s - T_f\right) \tag{8}$$

where $a_{sf} = A_{sf}/(A_b\ \Delta x)$ is interfacial area per unit of volume in the porous fin and h_{sf} is the convective heat transfer coefficient between solid and fluid phases in porous fin. Both a_{sf} and h_{sf} depend on the porous medium and their evaluations are given in open literature (see for example [2,3,106,112]).

Using the heat conduction Fourier law and Rosseland diffusion model, to estimate internal radiation effects, the local heat fluxes of the fluid and solid phases are written as [2,112]:

$$\dot{q}_f(x) = -\varphi k_f \frac{dT_f}{dx};\ \dot{q}_s(x) = -(1-\varphi)k_s \frac{dT_s}{dx} - \frac{4\sigma}{3\beta_R}\frac{dT_s^4}{dx} \tag{9}$$

where β_r is the Rosseland mean extinction coefficient.

By considering Eq. (9) and the linearized expression of T_s^4 around ambient temperature T_∞, Eqs. (7) and (8) can be written as:

$$\varphi k_f \frac{d^2 T_f}{dx^2} = h_{sf} a_{s,f}\left(T_f - T_s\right) + \frac{\rho_f c_{pf} g K \beta}{\nu t}\left(T_f - T_\infty\right)^2 \tag{10}$$

$$\left[(1-\varphi)k_s + \frac{16\sigma T_\infty^3}{3\beta_R}\right]\frac{d^2 T_s}{dx^2} = \left[\frac{h_L P(1-\varphi)}{A_b} + \frac{4P\sigma\varepsilon T_\infty^3}{A_b}\right](T_s - T_\infty) + h_{sf} a_{s,f}\left(T_s - T_f\right) \tag{11}$$

Equations (10) and (11) represent a second order system of nonlinear ordinary differential equations. The boundary conditions associated with Eqs. (10) and (11) are the following:

$$\begin{aligned} &T_f(0) = T_s(0) = T_b \text{ at base fin} \\ &\frac{dT_f}{dx}(L) = \frac{dT_s}{dx}(L) = 0 \text{ at tip fin} \end{aligned} \tag{12}$$

In dimensionless form, the energy equations (10) and (11) and the boundary conditions (12) are written as:

$$\frac{d^2\theta_f}{dX^2} = \chi Bi\left(\theta_f - \theta_s\right) + \frac{Ra^*}{\tau^2}\theta_f^2 \tag{13}$$

$$[1 + 4R_d]\frac{d^2\theta_s}{dX^2} = \frac{2}{\tau}(\lambda + R_1)\theta_s + Bi\left(\theta_s - \theta_f\right) \tag{14}$$

and:

$$\theta_f(0) = \theta_s(0) = 1;\ \frac{d\theta_f}{dx}(1) = \frac{d\theta_s}{dx}(1) = 0 \tag{15}$$

where the employed dimensionless variables are:

$$\begin{aligned} X = \frac{x}{L};\ \theta = \frac{T - T_\infty}{T_b - T_\infty};\ \tau = \frac{t}{L};\ \frac{PL}{A_b} \simeq \frac{2}{\tau};\ R_d = \frac{4\sigma T_\infty^3}{3\beta_R(1-\varphi)k_s}; \\ Ra^* = \frac{g\beta K(T_b - T_\infty)t}{\varphi\nu_f\alpha_f};\ \lambda = \frac{h_L L}{k_s};\ R_1 = 4\frac{\sigma\varepsilon T_\infty^3 L}{(1-\varphi)k_s}; \\ Bi = \frac{h_{sf} a_{s,f} L^2}{(1-\varphi)k_s};\ \chi = \frac{(1-\varphi)}{\varphi}\kappa;\ \kappa = \frac{k_s}{k_f} \end{aligned} \tag{16}$$

The average Nusselt numbers of the fluid and solid matrix are defined as follow:

$$Nu_f = \frac{\dot{q}_{f,b} t}{k_{eq}(T_b - T_\infty)} = -\frac{\varphi\tau}{\varphi + (1-\varphi)\kappa}\theta_f'(0) \tag{17}$$

$$Nu_s = \frac{\dot{q}_{s,b} t}{k_{eq}(T_b - T_\infty)} = -\frac{(1-\varphi)\kappa\tau}{\varphi + (1-\varphi)\kappa}(1 + 4R_d)\theta_s'(0) \tag{18}$$

and the total Nusselt number of the porous fin is:

$$Nu_t = \frac{\left(\dot{q}_{f,b} + \dot{q}_{s,b}\right)t}{k_{eq}(T_b - T_\infty)} = Nu_f + Nu_s \tag{19}$$

where $\dot{q}_{f,b}$ and $\dot{q}_{s,b}$ are the heat fluxes of the fluid and solid at base fin, respectively. The value of k_{eq} depends on the porous medium as pointed out in [2,3,106,112]. In the present investigation $k_{eq} = \varphi k_f + (1-\varphi)k_s$ is used as the effective thermal conductivity of porous fin, as given in [11,54].

3. Solution by Adomian decomposition method

The system of nonlinear differential equations given in Eqs. (13) and (14) along with the boundary conditions may not be solved with the common analytical technique. In the present work the Adomian decomposition method (ADM) [113,114] is applied to obtain a semi-analytical solution of the system of ordinary differential equations. For this purpose, it is convenient to write Eqs. (13) and (14) in the compact form, with $X = L\text{-}x$:

$$L_X\theta_s = \alpha\theta_s - \beta\theta_f \tag{20}$$

$$L_X\theta_f = \left(\delta\theta_f + \gamma\theta_f^2\right) - \delta\theta_s \tag{21}$$

where:

$$\beta = \frac{Bi}{(1 + 4R_d)};\ \alpha = \frac{2(\lambda + R_1)}{\tau(1 + 4R_d)} + \beta;\ \delta = \chi Bi;\ \gamma = \frac{Ra^*}{\tau^2} \tag{22}$$

and L_X is the linear second order differential operator ($L_X = d^2/dX^2$, with $X = L\text{-}x$). Assuming the inverse operator L_X^{-1} exists, it is defined as:

$$L_X^{-1}(\bullet) = \int_0^X \int_0^\xi (\bullet)\, d\zeta\, d\xi \tag{23}$$

Applying the inverse operator to Eqs. (20) and (21) and using the boundary conditions (15), the followings obtain:

$$\theta_s(X) = \theta_{0,s} + \alpha L_X^{-1}\theta_s - \beta L_X^{-1}\theta_f \tag{24}$$

$$\theta_f(X) = \theta_{0,f} + \left(\delta L_X^{-1}\theta_f + \gamma L_X^{-1}\theta_f^2\right) - \delta L_X^{-1}\theta_s \tag{25}$$

where:

$$\theta_{0,s} = \theta_s(0);\ \theta_{0,f} = \theta_f(0) \tag{26}$$

are the unknown temperatures for the fluid and solid at the tip of the fin. These temperatures are determined by applying the boundary conditions (15). In the ADM the solution θ and the nonlinear term $N = \theta^2$, are expressed as:

$$\theta = \sum_{n=0}^{\infty} \theta_n;\ N(\theta) = \sum_{n=0}^{\infty} A_n \tag{27}$$

where A_n are the Adomian polynomials, which can be determined by [113]:

$$A_n = \frac{1}{n!}\left[\frac{d^n}{d\lambda^n} N\left(\sum_{n=0}^{\infty} \lambda^n \theta_n\right)\right] \tag{28}$$

Inserting the decomposition series (27) into equations (24) and (25), they yield:

$$\sum_{n=0}^{\infty} \theta_{n,s} = \theta_{0,s} + \alpha L_X^{-1} \sum_{n=0}^{\infty} \theta_{n,s} - \beta L_X^{-1} \sum_{n=0}^{\infty} \theta_{n,f} \tag{29}$$

$$\sum_{n=0}^{\infty} \theta_{n,f} = \theta_{0,f} + \left(\delta L_X^{-1} \sum_{n=0}^{\infty} \theta_{n,f} + \gamma L_X^{-1} \sum_{n=0}^{\infty} A_n\right) - \delta L_X^{-1} \sum_{n=0}^{\infty} \theta_{n,s} \tag{30}$$

where $\theta_{f,n}$ and $\theta_{s,n}$ are Adomian polynomials referring to the fluid and solid energy equations, respectively. Now according to ADM, we can obtain the components $\theta_{f,n}$ and $\theta_{s,n}$ recursively as follows:

$$\theta_{n,s} = \alpha L_X^{-1} \theta_{n-1,s} - \beta L_X^{-1} \theta_{n-1,f} \tag{31}$$

$$\theta_{n,f} = \delta L_X^{-1} \theta_{n,f} + \gamma L_X^{-1} A_{n-1} - \delta L_X^{-1} \theta_{n-1,s}\ n \geqslant 1 \tag{32}$$

where $\theta_{f,0}$ and $\theta_{s,0}$ are given by (27) and A_n, for $N(\theta) = \theta^2$, results in (Appendix A):

$$A_n = \sum_{k=0}^{n} \theta_{k,f} \theta_{n-k,f}\ ,\ n \geqslant 0 \tag{33}$$

By processing the inverse operator L_X^{-1} into Eqs. (31) and (32), taking into account the expression (33), the following approximate analytical solutions for the temperatures of the fluid and of solid are obtained (Appendix B):

$$\theta_s(X) = \sum_{n=0}^{m} \widetilde{\theta}_{n,s} X^{2n} \tag{34a}$$

$$\theta_f(X) = \sum_{n=0}^{m} \widetilde{\theta}_{n,f} X^{2n} \tag{34b}$$

where the coefficients $\widetilde{\theta}_{n,f}$ and $\widetilde{\theta}_{n,s}$ of the series (34) are solutions of the following system of the nonlinear algebraic equations:

$$\begin{cases} \widetilde{\theta}_{0,s} = \theta_{0,s};\ \widetilde{\theta}_{0,f} = \theta_{0,f} \\ \widetilde{\theta}_{n,s} = \dfrac{1}{2n(2n-1)}\left(\alpha \widetilde{\theta}_{n-1,s} - \beta \widetilde{\theta}_{n-1,f}\right) \\ \widetilde{\theta}_{n,f} = \dfrac{1}{2n(2n-1)}\left[\delta\left(\widetilde{\theta}_{n-1,f} - \widetilde{\theta}_{n-1,s}\right) + \gamma\left(\sum_{k=0}^{n-1} \widetilde{\theta}_{k,f} \widetilde{\theta}_{n-1-k,f}\right)\right]^n \\ \sum_{n=0}^{m} \widetilde{\theta}_{n,s} = 1;\ \sum_{n=0}^{m} \widetilde{\theta}_{n,f} = 1 \end{cases} = 1, 2, \ldots m \tag{35}$$

System (35) is formed by the $2(m + 1)$ nonlinear equations with $2(m + 1)$ unknowns and it can be solved by Newton-Raphson iterative method [115].

3.1. Verification and validation

The ADM employed to evaluate solution of the mathematical problem of ODE, with the assigned boundary conditions described in Eqs. (13)-(15) is verified and validated. The verification is the convergence study of the series (34) and it is accomplished by evaluating the increase in the accuracy of the solution increasing the number of the series terms in Eq. (34). The validation is carried out by means of comparison between the solution with ADM and the solution carried out by the finite difference method (FDM), and the results provided by Kiwan [12].

The analysis of the series convergence, Eq. (34), is achieved for a porous fin with Ra^*=50, $Bi = 1$ and 100, $R_d = 0.1$, $R_1 = 0.3$, $\lambda = 0$, $\kappa = 1000$ and $\varphi = 0.92$. It should be highlighted that $\kappa = 1000$ points out a very high difference between the solid and fluid thermal conductivities whereas $Bi = 1$ and 100 indicate a low or high convective heat transfer inside the porous fin between the solid and fluid phases. In Fig. 2, the dimensionless fluid and solid phase temperature distributions are shown for different number of terms, n, of the series (34). It is observed that as the number of terms "n" increases, the dimensionless temperature of both solid and fluid tend towards an asymptotic distribution. The asymptotic temperature profiles of the fluid and solid phases are attained for $n = 121$. Convergence of fluid temperature profiles is slower than the solid temperature profiles due to the higher thermal conductivity of the solid. It is interesting to observe that the lower thermal conductivity in the fluid phase determines a high temperature gradient close to the base of the fin.

In Fig. 3, Nusselt number as a function of Ra^* for different values of n is reported for $Bi = 1.0$ and 100, Fig. 3a and 3b, respectively. It is observed that the error of the solution evaluated for an assigned n value with respect to the asymptotic solution increases as Ra^* increases, and the differences are greater for $Bi = 1$ than for $Bi = 100$. In Fig. 3a for $Bi = 1.0$, the solution for $n = 7$ converges to the asymptotic one for $Ra^*<1$, whereas for $Bi = 100$, the solution for $n = 7$ approaches to the asymptotic solution (for $n = 241$) for $Ra^*<12$. It implies that, the weaker the convergence, the greater the Ra^* and the smaller the Biot number. In the following the results are evaluated for the number of series terms, n, equal to 61 because it represents a good compromise between the computational time and accuracy of the solution. It should be underlined that the Nusselt number is due to the results of the heat transfer inside the porous medium between the fluid and solid. The fluid penetrates inside the porous fin at T_∞; in this way the Nusselt number is the total heat transfer between the surface at temperature T_b and the fluid at ambient temperature T_∞ by means of the porous fin.

In Fig. 4, the temperature profiles carried out by the FDM with different nodes are given for fluid and solid matrix, Fig. 4a and 4b, respectively, together with the ones evaluated with ADM with $n = 61$, Ra^*=50, $Bi = 1.0$, $\kappa = 10^3$ are given. It is observed that by increasing the number of nodes, the temperature variations are greater for the fluid, in Fig. 4a, than for the solid matrix, in Fig. 4b. Indeed, the temperature profile of the solid matrix, Fig. 4b, changes very slightly and coincides with the analytical solution achieved with ADM, whereas the fluid temperature profile, evaluated by the FDM, coincides with the one carried out by the ADM with $n = 61$. The percentage errors of the maximum fluid temperature difference as n varies with respect to the asymptotic value of the semi-analytical solution are 12% for $n = 25$, 2.5% for $n = 51$ and<0.75% for $n = 101$.

The comparison between the total Nusselt number of the model developed under LTNE conditions and the Nusselt number of the infinite fin under LTE conditions developed by Kiwan [12] is shown in Fig. 5. It is accomplished for $Bi = 10^6$, $\tau = 0.05$, $\varphi = 0.92$, $\kappa = 1.0$, $\lambda = R_1 = 0$. In this case, the internal heat transfer due to the interstitial convective heat transfer is very high with respect to the conduction inside the solid and this allows for LTNE solution to tend towards the LTE one. The present model of porous fin with finite length developed with LTNE model reaches the porous fin with infinite length developed in LTE model for Bi and τ tending to the infinite. The convective thermal resistance on the

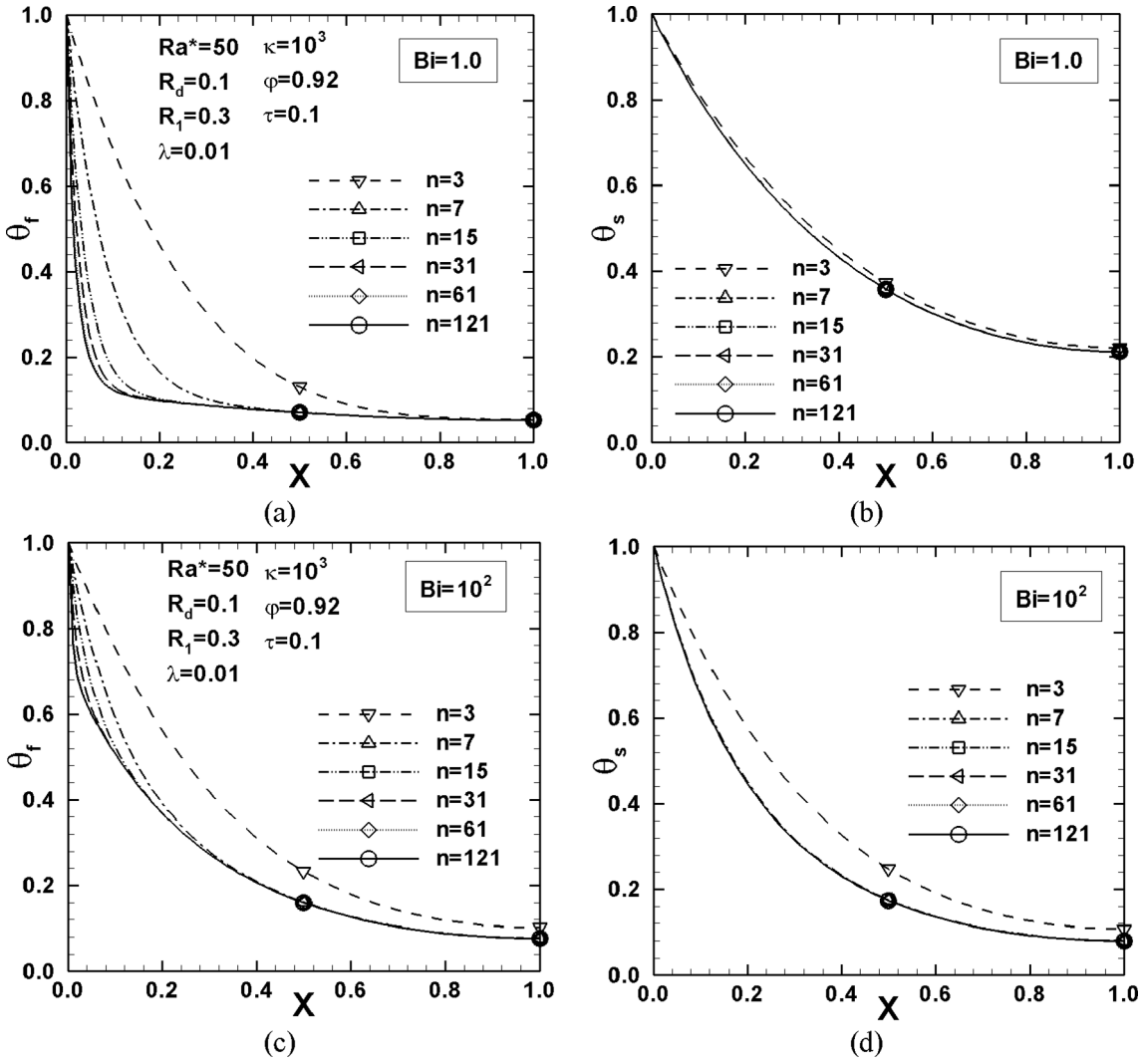

Fig. 2. Analytical solution for Ra^*=50, $Bi = 1$ and 100, $R_d = 0.1$, $R_1 = 0.3$, $\lambda = 0$, $\kappa = 1000$ and $\varphi = 0.92$ with different number of terms *"n"* in the Adomian series: (a) Bi = 1.0 and θ_f, (b) Bi = 1.0 and θ_s (c) Bi = 10^2 and θ_f, (d) Bi = 10^2 and θ_s.

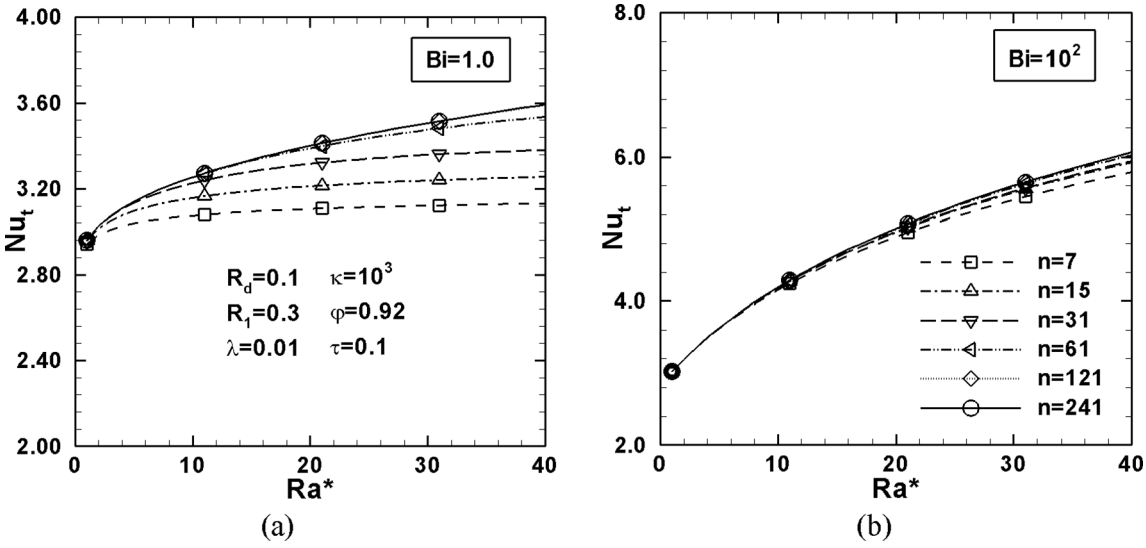

Fig. 3. Total Nusselt number as a function of Ra* for various number of series terms*"n"* and for: (a) Bi = 1.0; (b) Bi = 100.

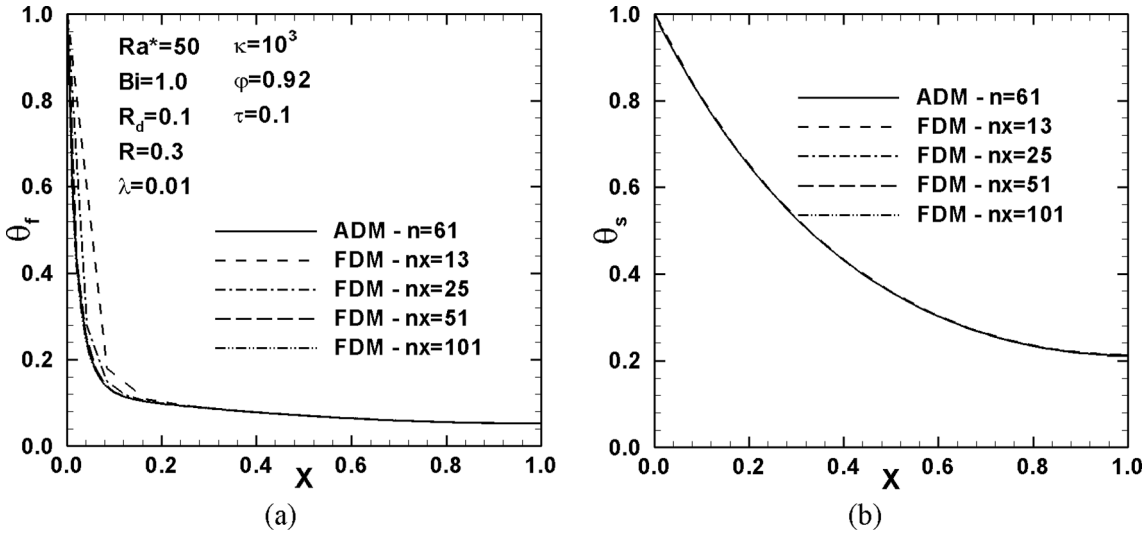

Fig. 4. Comparison between the solution given by ADM for n = 61 and solutions carried out by means of the FDM with different nodes: (a) fluid temperature profiles, (b) solid temperature profiles.

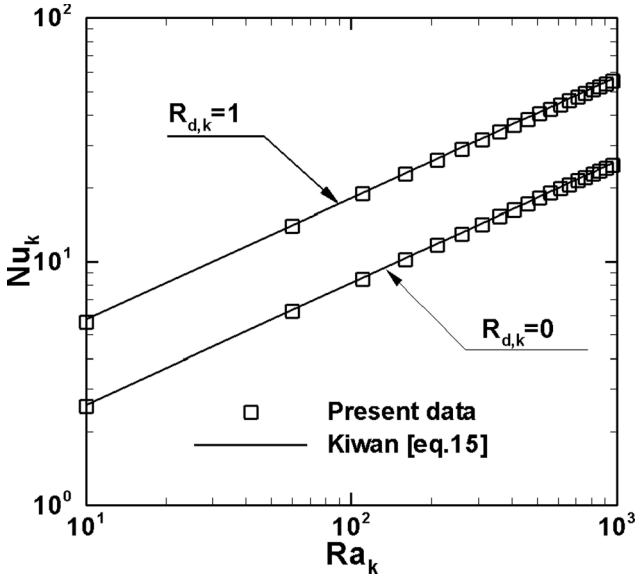

Fig. 5. Comparison between the results of present investigation and the ones of Kiwan [12]. In the present investigation the input parameters are: Bi = 10^6, τ = 0.05, φ = 0.92, κ = 0.1 , R_1 = λ = 0.

fluid solid interface for $Bi \to \infty$ is very small and the average temperatures of the fluid and the solid on the representative elementary volume (REV) coincide, i.e. $T_f = T_s$. In Fig. 5, the comparison is given in terms of the Nusselt number, Nu_k, given in Eq. (15) reported by Kiwan [12] as a function of Ra_k, where $Nu_k = \tau Nu_t$ and $Ra_k = (\varphi k_f / k_{eq})\ Ra^*$, for two values of $R_{d,k}$ equal to 0 and 1.0, with $R_{d,k} = R_d\,(1\text{-}\varphi)\,k_s/k_{eq}$. It is observed that the values given by Kiwan [12] and the present data are in harmony.

4. Results and discussion

The results obtained with the Adomian decomposition method (ADM) applied to the energy equations of finite length fin with adiabatic tip are shown and discussed below, under the hypothesis of local thermal non-equilibrium (LTNE) between the fluid and the solid phases. The results are presented as dimensionless temperature profiles for the fluid and solid phases along the porous fins and in terms of total Nusselt number. The following are the dimensionless parameter ranges: $0 \le Ra^* \le 10^3$, $1 \le Bi \le 10^6$, $0 \le R_1 \le 0.05$; $0 \le R_d \le 1.0$, $0.01 \le \tau \le 0.1$, $0 \le \lambda \le 1.0$, $0.6 \le \varphi \le 0.95$, $1.0 \le \kappa \le 10^4$.

4.1. Convective effects: Biot and Rayleigh numbers and external convective heat transfer coefficient effects on temperature profiles

Temperature profiles of fluid and solid phases along the dimensionless coordinate X are reported in Fig. 6a and 6b, respectively, for Bi = 1.0, 10^2, 10^3 and 10^6, which indicate from low to high convective heat transfer with respect to the conduction in the solid phase. The other parameters are $\kappa = 10^4$, with a very high different thermal conductivity values which determine a high temperature difference between fluid and solid phases. This could be the case of porous fin in aluminum with air as fluid and a negligible external convective heat transfer, $\lambda = 0$. Temperature profiles of fluid and solid decrease along the longitudinal axis X and, consequently as expected, the longitudinal conductive effects decrease along the axis of the porous fin. As the Biot number increases, fluid temperature increases while solid matrix temperature decreases. This implies that the temperature difference between solid and fluid phases, decreases as the Bi value increases. In fact, as the Biot number increases, the convective conductance on the fluid–solid interface of the porous medium increases with a consequent improvement of volumetric heat exchange between the solid matrix and the fluid and a reduction of the temperature difference between solid and fluid. For Bi = 1.0, the conductive effect is dominant and, consequently, for high κ (=10^4) a high gradient temperature is detected for the fluid phase at the fin base. For $Bi \ge 10^3$, the temperature profiles of the fluid and the solid are practically coincident. Therefore, the solid matrix and the fluid have attained a condition of local thermal equilibrium (LTE). The heat is directly transferred in the solid and the thermal resistance globally decreases.

Temperature profiles of fluid and solid along the axis of the porous fin for different values of the Rayleigh number, Ra^* = 1, 10^2,5x10^2 and 10^3, are shown in Fig. 7. As Ra^* increases, temperature profiles of fluid and solid matrix tend more rapidly to the surrounding environment temperature. The porous fin allows to remove a greater heat transfer rate from the base where the fin is placed on the surface. This can be explained observing that the Rayleigh number, Ra^*, depends on the permeability of the porous medium, for assigned temperature difference between the fin base, T_b, and the ambient, T_∞. An increase in Ra^* means a greater permeability of the fluid through the solid matrix, with a consequent increase in heat transfer by buoyancy.

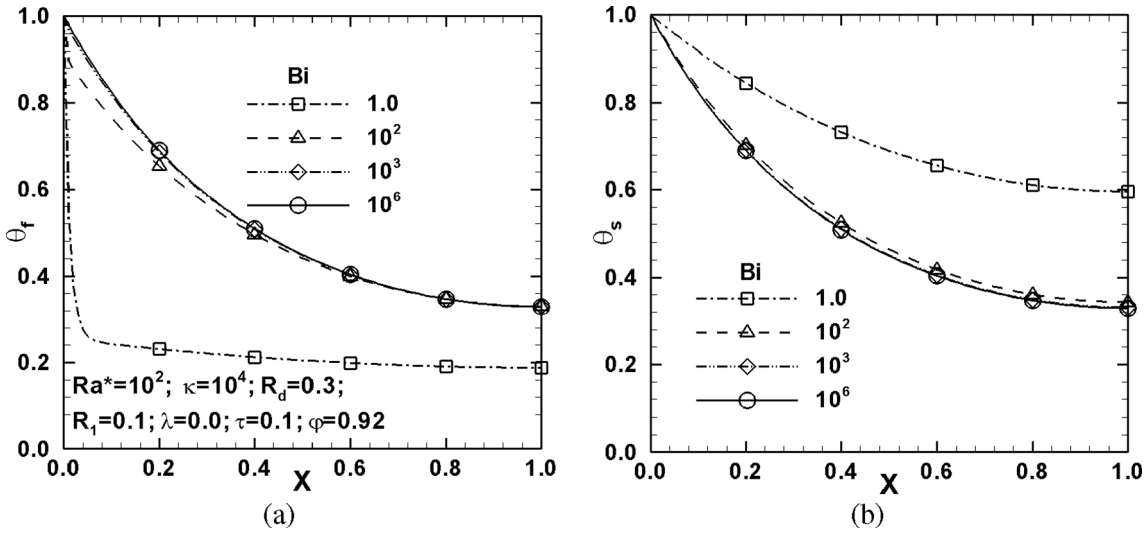

Fig. 6. Temperature profiles along the porous fin for Bi = 1.0 ÷ 10^6: (a) fluid temperatures (b) solid temperatures.

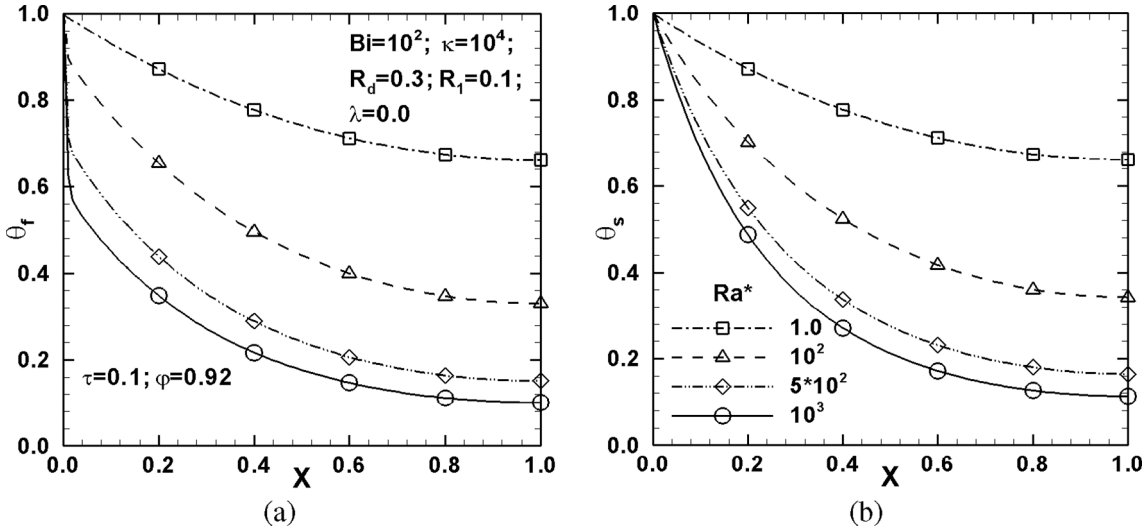

Fig. 7. Temperature profiles along the porous fin for Ra*=1.0 ÷ 10^3: (a) fluid temperatures (b) solid temperatures.

The dependence of the fluid temperature and the solid temperature profiles on Ra^*, for different Bi, is reported in Fig. 8. In Fig. 8a, for Bi = 1.0, the differences between the temperatures of the fluid and the solid increase as the Rayleigh number, Ra^*, increases. They decrease as the Biot number increases, as shown in Fig. 8b and 8c. This indicates that at greater Rayleigh number, the local thermal equilibrium (LTE) between the solid matrix and the fluid is achieved for much higher Biot numbers. In local thermal equilibrium (LTE) conditions, the decrease in the dimensionless temperature as the Ra^* parameter increases is also confirmed in [12,116].

The effect of the external convective heat transfer parameter, λ, on the temperature profiles is depicted in Fig. 9, for $Ra^* = 10^2$ and Bi equals to 10 and 10^4. In Fig. 9a and 9b, the fluid and solid temperatures decrease as the external convective heat transfer parameter λ increases. This is due to the increase in convective heat transfer toward external fluid ambient which determines the decrease of solid temperature along the fin and, consequently, the decrease in the fluid temperature along the porous fin. Moreover, for Ra^*=100 and $Bi = 10^4$, in Fig. 9b, the solid matrix and the fluid show the same temperature values, and they attain the local thermal equilibrium condition.

4.2. Internal and external radiation effects on temperature profiles

The effect of internal radiation parameter, R_d, on temperature distribution inside the fin, for Ra^*=10 and Bi equal to 10, 10^2, 10^4, is shown in Fig. 10. It is observed that for all Bi values, the increase in internal radiative parameter causes fluid and solid temperatures increase in the porous fin. Indeed, increase in internal radiation parameter R_d determines a lower radiative-conductive resistance of the porous fin and, consequently, the temperature tends to be more uniform along the fin and closer to the base temperature according to Banja et al. [116]. Furthermore, temperature differences between solid and fluid phases, as the internal radiative parameter varies, are more marked for Bi = 10 than for $Bi = 10^2$, while for $Bi = 10^4$, the solid and fluid temperature profiles are practically equal for all values of the internal radiative parameter R_d. For all R_d values, considered in the present analysis, and high Biot number value, 10^4, the LTE assumption is acceptable.

Effects of the external radiation parameter, R_1, on temperature distribution are shown in Fig. 11, for $Ra^* = 10^2$ and Bi equal to 10 and 10^4. It can be seen, from Fig. 11a and 11b that both the solid temperature and the fluid temperature decrease as the external radiative parameter R_1 increases. In fact, as R_1 increases, the radiative heat transfer of the solid matrix towards the external environment increases and, therefore, the

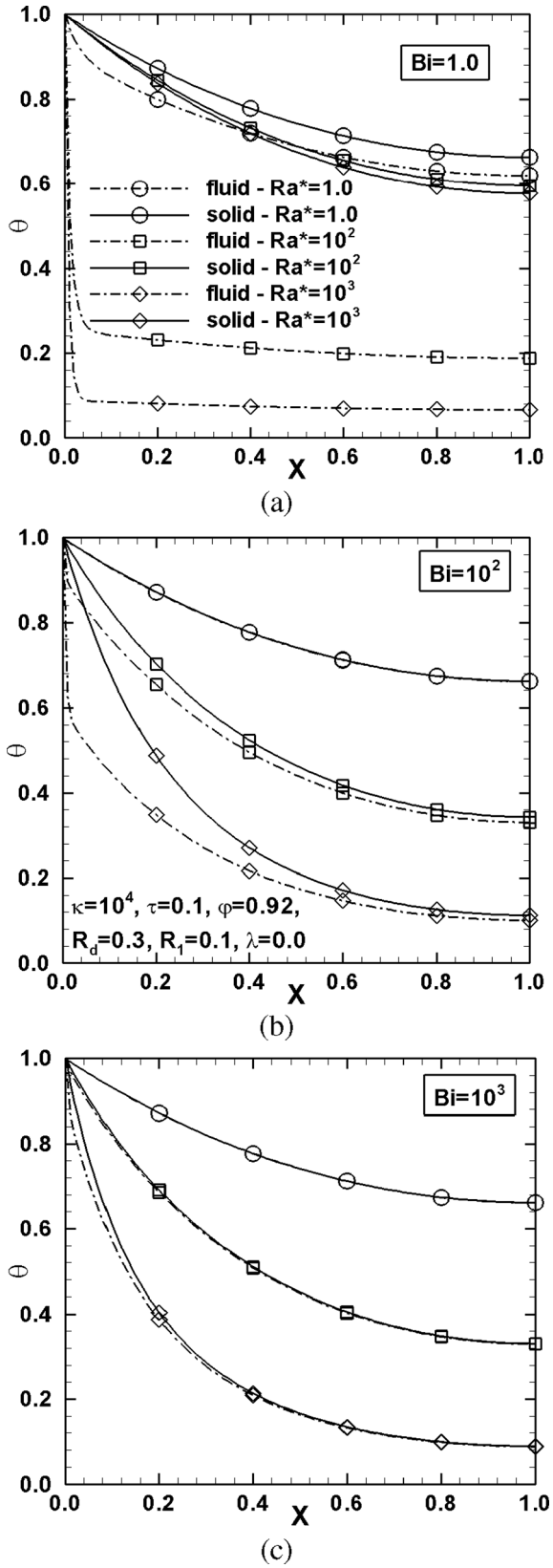

Fig. 8. Fluid and solid phase temperature profiles along the porous fin for Ra*=1.0 ÷ 10^3: (a) Bi = 1.0 (b) Bi = 10^2 (c) Bi = 10^3.

solid temperature along the fin decreases as well as the fluid temperatures decreases. It is also observed that, in Fig. 11b for Ra^*=100 and $Bi = 10^4$, the solid matrix and the fluid are in local thermal equilibrium condition and the temperatures decrease to the same amount as the radiative parameter R_1 increases, in accordance with Banja et al. [116].

4.3. Conductive and geometrical effects on temperature profiles

Fluid and solid temperature profiles along the longitudinal axis of the porous fin are reported in Fig. 12 for different thermal conductivity ratios, $\kappa = 10$ (carbon foam - air), $\kappa = 100$ (SiC foam -water) and $\kappa = 10^4$ (aluminum foam - air). In all the cases examined, it is noted that as the solid–fluid thermal conductivity ratio, κ, increases the solid and fluid temperature profiles tend towards higher temperature values. This is because an increase in the thermal conductivity ratio is obtained by increasing the thermal conductivity of the porous matrix and consequently, the thermal conductive resistance of the solid decreases. The reduction in conductive thermal resistance determines the solid temperature increases and, consequently, that of the fluid temperature. Moreover, temperature differences between fluid and solid decrease as the thermal conductivity ratio increases κ and the Biot number increases, as pointed out in Fig. 12a and 12b. This is due to the lower thermal resistance inside the porous fin.

The differences between fluid and solid temperature profiles, for assigned Biot number value, 10^2, and different thermal conductivity ratios, increase as the Rayleigh number increases, as indicated in Fig. 13, where the temperature profiles are given for Ra^*=1.0 and Ra^*=10^2, Fig. 13a and 13b, respectively. For lower Ra^* value equated to 1.0, in Fig. 13a, the differences between the two profiles, for fluid and solid, decrease significantly and disappear for very high thermal conductivity ratio, $\kappa = 10^4$. In these cases, the diffusive effect prevails on the convective one due to the buoyancy and the temperature difference between the base and tip of the fin is lower. For lower κ value, the temperature gradient along the fin increases due to the decrease in diffusive effect with respect to the buoyancy effect. For higher Ra^* value, 10^4, the buoyancy effect is higher than the one in the previous case and for the same κ value it causes higher temperature gradient inside the fin. It is interesting to observe that for all Rayleigh numbers and thermal conductivity ratio values, the temperature differences between the fluid and solid tend towards zero for $X > 0.8$, as shown in Fig. 13. This is due to the exhaust heat transfer between solid and fluid phases inside the fin and between the porous fin and the ambient.

The geometric parameter ($\tau = t/L$) effect on solid and fluid temperature profiles is shown for $Bi = 10$ and $Bi = 10^4$ in Fig. 14a and 14b, respectively. Decrease in the geometric parameter $\tau = t/L$ can be obtained either with a reduction in the thickness, t, for assigned fin length, L, or with an increase in the fin length, for assigned fin thickness. In Fig. 14a and 14b, it is observed that as the geometric parameter τ increases, the temperature of the fin tip increases as well. In fact, close to the base temperature, for a given thickness t of the fin, the temperature is much higher the smaller the length of the fin. Furthermore, in Fig. 14a, for $Bi = 10$, the temperature differences between solid and fluid increase as the fin aspect ratio decreases. The increase in the fin aspect ratio, for assigned fin length, determines a higher thickness and a lower thermal resistance of the fin. Consequently, lower temperature gradient is attained at the fin base for both solid and fluid phases.

4.4. Total Nusselt number profiles

The total Nusselt number profiles as a function of the Rayleigh number are reported in Fig. 15, for dimensionless parameter ranges $1 \leq Bi \leq 10^4$, in Fig. 15a, $1.0 \leq \kappa \leq 10^4$, in Fig. 15b, $0 \leq R_d \leq 1.0$, in Fig. 15c, and $0.01 \leq \tau \leq 0.1$, in Fig. 15d.

The Nusselt number increases as the Ra^* increases for all cases examined, as shown in Fig. 15. In fact, as the Rayleigh number increases, the mass flow rate induced by the buoyancy force increases, and

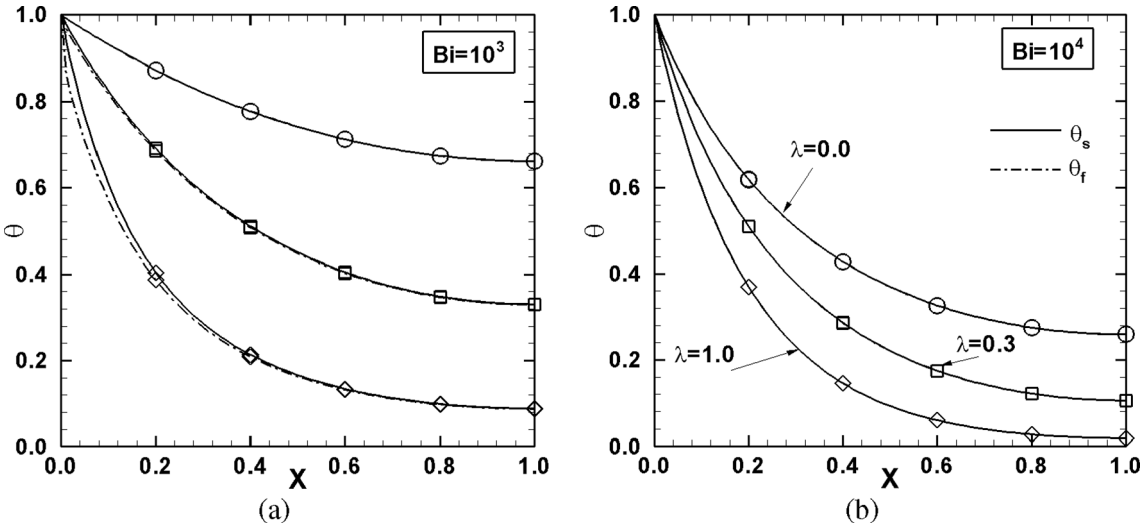

Fig. 9. Fluid and solid phase temperature profiles along the porous fin for λ = 0.0, 0.3 and 1: (a) Bi = 10 (b) Bi = 10^4.

consequently, the heat transfer removed from the porous fin increases. It is observed, in Fig. 15a, that the values of the total Nusselt number are greater as the Biot number increases. As the Biot number increases, the Nu_t profiles tend towards an asymptotic profile that corresponds to the local thermal equilibrium (LTE) condition which occurs for $Bi = 10^4$. Actually, as the convective heat transfer coefficient on the solid matrix - fluid interface increases, the Biot number increases, leading to an increase in the heat transfer rate removed from the base of the fin. Therefore, the local thermal equilibrium (LTE) assumption, which has been considered in the literature, involves an overestimation of the Nusselt number compared to the local thermal non-equilibrium (LTNE) assumption.

The effect of the fluid–solid thermal conductivity ratio, κ, on the total Nusselt number is shown in Fig. 15b for $Bi = 10^2$, $\tau = 0.1$, $\varphi = 0.92$ e $R_d = R_1 = \lambda = 0$. It is observed that the total Nusselt number, for a given Ra^* value, decreases with the increase of the thermal conductivity ratio. As the ratio of thermal conductivities between fluid and solid increases, which is achieved for metal fins (Al, Cu), the thermal resistance of the solid matrix decreases and therefore the temperature of the fin tends towards the base temperature. Since, in Fig. 15b, R1 $= R_d = \lambda = 0$, the heat transfer rate removed from the porous matrix decreases.

In Fig. 15c the effect of the dimensionless internal radiative parameter, R_d, on the Nusselt number, Nu_t, is reported for $Bi = 10^2$, $\kappa = 10^4$, $\tau = 0.1$, $\varphi = 0.92$ e $R_1 = \lambda = 0$. The dimensionless internal radiative parameter, R_d, increases as the radiative heat exchange inside the porous matrix increases. As the parameter R_d increases, the heat transfer rate removed from the base of the porous fin increases and therefore the total Nusselt number increases, as observed in Fig. 15c.

The effect of the aspect ratio of the porous fin on the total Nusselt number, Nu_t, is given in Fig. 15d for $Bi = 10^2$, $\kappa = 10^4$, $\varphi = 0.92$ e $R_1 = R_d = \lambda = 0$. The Nu_t is lower for $\tau = 0.1$ than the one for $\tau = 0.01$ up to Ra^* about 6. For $\tau = 0.03$ and 0.05 the reversal of trend, with respect to the value for $\tau = 0.1$, starts with Ra^* equal about 18 and 27, respectively. For Ra^* values higher than 27, temperature differences between the base and the ambient become higher, and for fins with lower length temperature exhibits higher values. Consequently, the higher the value of τ, the greater the heat transfer rate. The different trends can be explained taking into account the heat transfer rate from the porous fin. It is related to the external heat transfer surface and the temperature difference between the fin base and ambient temperatures. Low Ra^*, for assigned thickness, means low temperature differences between the base and the ambient and the heat transfer area is the most important term. For low dimensionless thickness, τ, the fin length, L, is high as well as the heat transfer area. It should be noted that for $\tau = 0.01$ the total Nusselt number tends to an asymptotic value of about 0.08. In fact, for $\tau = 0.01$ the fin tends towards the infinitely long fin ($\tau \to 0$) characterized by a large area with a temperature close to ambient temperature and with invariably zero heat transfer. For aspect ratio values $\tau \geq 0.03$, the Nusselt number does not attain an asymptotic value for the considered Ra^* values.

4.5. Conditions for local thermal equilibrium in porous fins

The assumption of local thermal equilibrium (LTE) can be considered applicable when the difference in the average temperature, in the representative elemental volume (REV), between the fluid and solid phases is negligible, i.e. $T_f \cong T_s$. In practice, the hypothesis of local thermal equilibrium (LTE) can be considered valid for [102,103,105-107,112,117]:

$$\Delta T_l \ll \Delta T_L \tag{36}$$

where ΔT_L is the temperature difference on the system length scale and ΔT_l is the temperature difference between the solid phase and the fluid phase in the representative elemental volume (REV) of the porous medium or local scale length. The temperature difference on the fin length scale is equal to $\Delta T_L = T_b\text{-}T_\infty$ while the temperature difference on the local length scale is equal to $\Delta T_l = T_s\text{-}T_f$.

Differences in temperatures ΔT_L and ΔT_l are estimated with scale analysis. The heat transfer removed from the solid matrix at the base of the fin is transferred to the fluid and the external environment by means of buoyancy on the solid–fluid interface and external radiation and convection. Heat transferred from the solid matrix of the fin to the fluid is transported by the fluid due to the convection phenomenon. Neglecting the convective and radiative effects towards the outside, the energy balance, is:

$$\dot{Q}_f \approx \dot{Q}_{s,f} \tag{37}$$

The maximum convective heat transfer transported by the fluid is:

$$\dot{Q}_f \sim \dot{m} c_p \Delta T_L \tag{38}$$

while the heat transfer on the fluid solid interface is:

$$\dot{Q}_{s,f} \sim h_{s,f} A_{s,f} \Delta T_l \tag{39}$$

From Eqs. (37), (38) and (39) it results [117]:

$$\frac{\Delta T_l}{\Delta T_L} \sim \frac{\dot{m} c_p}{h_{s,f} A_{s,f}} \tag{40}$$

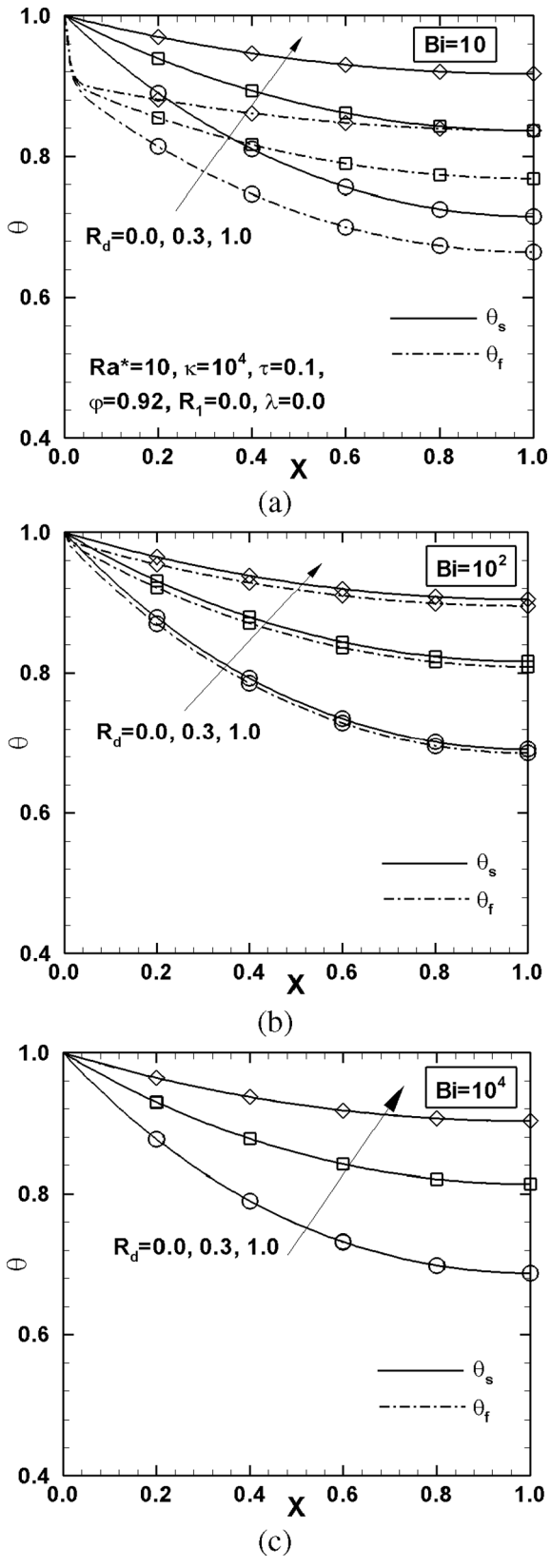

Fig. 10. Fluid and solid phase temperature profiles along the porous fin for R_d = 0.0, 0.3 and 1.0: (a) Bi = 10 (b) Bi = 10^2 (c) Bi = 10^4.

The order of magnitude of the mass flow rate induced by buoyancy effects, assuming Darcy model, can be estimated as follows:

$$\dot{m} \sim \rho \frac{gK\beta\Delta T_L}{\nu} WL \tag{41}$$

By replacing Eq. (41) with Eq. (40), it is:

$$\frac{\Delta T_l}{\Delta T_L} = |\theta_s - \theta_f| \sim \frac{\varphi Ra^*}{(1-\varphi)\kappa\tau^2 Bi} \tag{42}$$

where the dimensionless parameters Ra^*, Bi, θ, φ, κ and τ are defined in Eq. (18).

Ultimately, the hypothesis of local thermal equilibrium between the fluid and the solid matrix is obtained when:

$$\frac{\Delta T_l}{\Delta T_L} = |\theta_s - \theta_f| \sim \frac{\varphi Ra^*}{(1-\varphi)\tau^2(\kappa Bi)} \ll 1 \tag{43}$$

Equation (43) expresses a criterion for the local thermal equilibrium condition (LTE) of the porous fin as a function of global dimensionless parameters: buoyancy effects Ra^*, ratio of the thermal conductivity of the solid–fluid pair κ, porosity φ and of the heat transfer on the fluid–solid interface ($\kappa\, Bi$).

The criterion based on the semi analytical solution (ADM), to quantify the validity of the local thermal equilibrium hypothesis is defined as:

$$Err = \frac{max|T_s - T_f|}{\Delta T_L} = max|\theta_s - \theta_f| \tag{44}$$

The local thermal equilibrium (LTE) assumption can be considered valid when Err $\leq$ 0.05.

In Fig. 16, the maps (Ra^*, $\kappa\, Bi$) are reported in logarithmic scale, where the curves separate the zone of local thermal equilibrium (LTE) from the zone of local thermal non-equilibrium (LTNE). The comparison between the criterion for LTE obtained from the scale analysis, in Eq. (43), and the semi-analytical solutions by ADM, Eq. (44), are depicted in Fig. 16a. The comparison shows a good agreement between these two criteria. In Fig. 16a and 16b, it is observed that the condition of local thermal non-equilibrium (LTNE) becomes dominant the greater the effect of buoyancy, for higher Ra^*, and the lower the solid–fluid interface convection coefficient, for lower κBi. The increase in Ra^* also determines, for assigned Bi value, an increase in local temperature difference to obtain the same heat transfer between the fluid and solid phases. At assigned Ra^* value, the increase in Bi value allows to have a lower local temperature difference in order to realize the same heat transfer between solid and fluid phases inside the porous medium according to [106] in terms of Sparrow number. In Fig. 16b the effect of the conductivity ratio on the local thermal equilibrium (LTE) condition is shown. It is observed that the local thermal equilibrium is reached for lower values of κBi the lower the thermal conductivity ratio. The increase in κ, for assigned Ra^* value, causes an increase in κBi value. Moreover, at assigned κ the increase in Ra^* determines an increase in Bi value, i.e., an increase in local heat transfer coefficient between fluid and solid phases.

5. Conclusions

A simplified thermal model of porous fin of finite length with adiabatic tip under local thermal non-equilibrium assumption was proposed for the first time. An enlarged review of the previous investigations highlighted that only the local thermal equilibrium assumption was employed in earlier works. Initial analysis of two energy equations for porous fin was accomplished using the Adomian decomposition method. It focused on the thermal behaviors evaluating solid and fluid phase temperature profiles along the porous fin and the total Nusselt number in terms of geometrical and thermal parameters.

The main differences between solid and fluid temperature profiles as

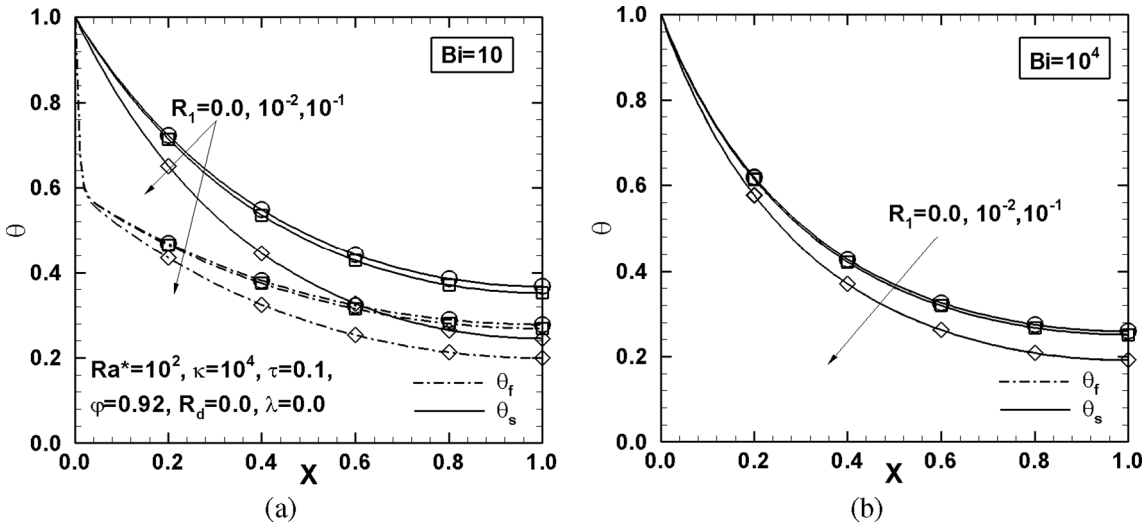

Fig. 11. Fluid and solid phase temperature profiles along the porous fin for $R_1 = 0.0$, 0.01 and 0.1: (a) Bi = 10 (b) Bi = 10^4.

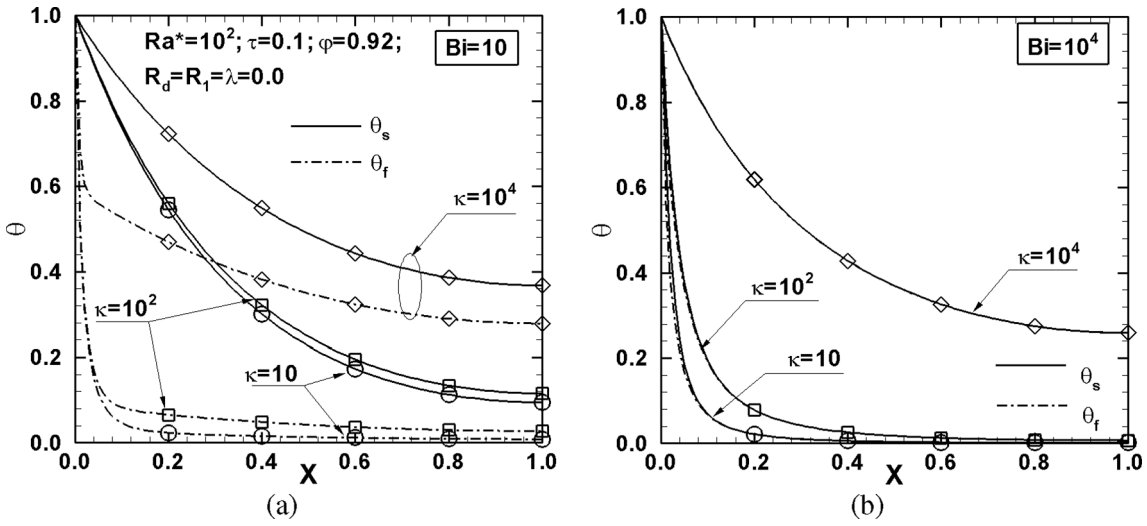

Fig. 12. Fluid and solid phase temperature profiles along the porous fin for Ra*=10^2 and $\kappa = 10$, 10^2 and 10^4: (a) Bi = 10 (b) Bi = 10^4.

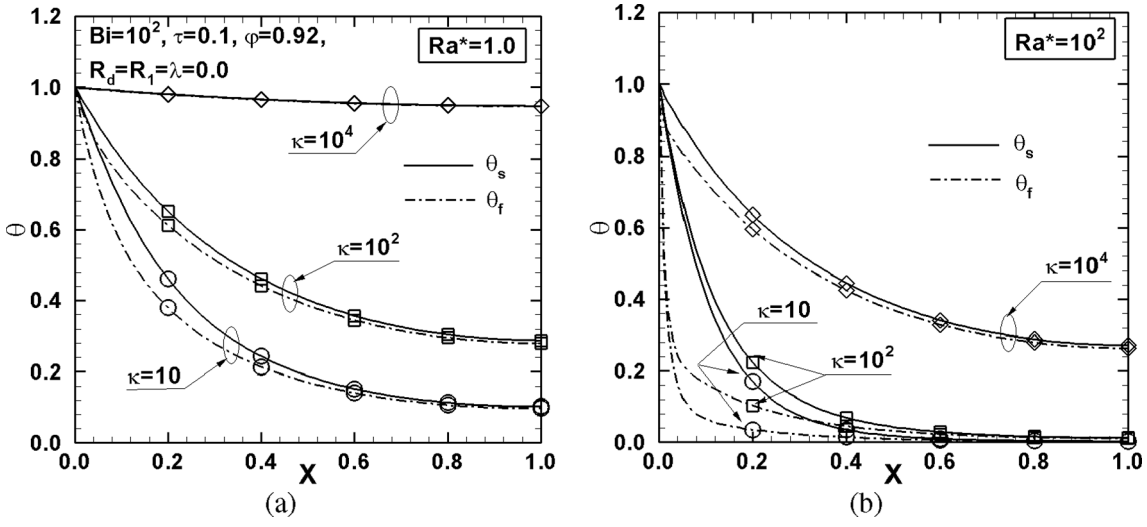

Fig. 13. Fluid and solid phase temperature profiles along the porous fin for Bi = 10^2 and $\kappa = 10$, 10^2 and 10^4: (a) Ra*=1.0 (b) Ra*=10^2.

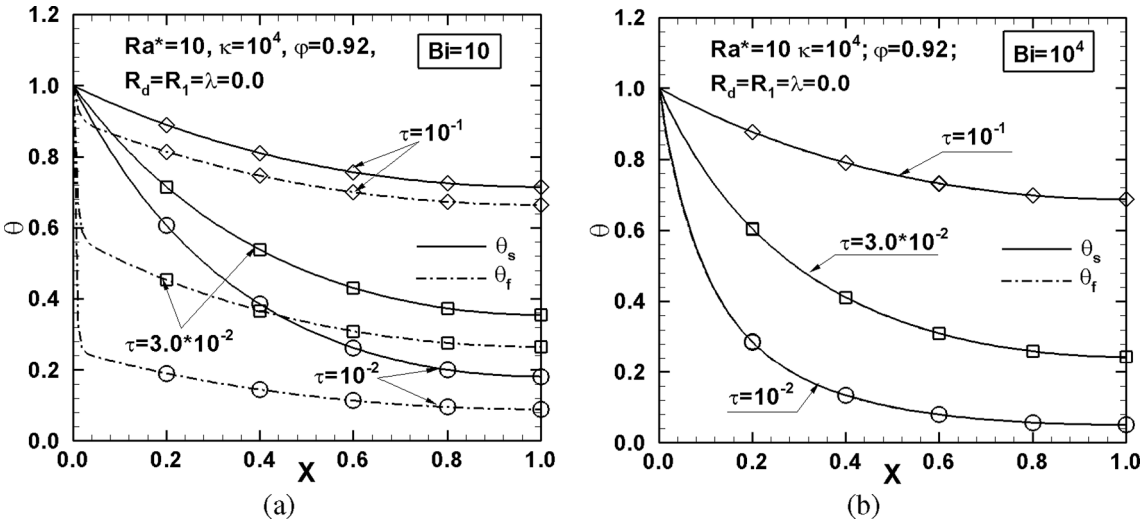

Fig. 14. Fluid and solid phase temperature profiles along the porous fin for $\tau = 10^{-2}$, $3.0x10^{-2}$ and 10^{-1}: (a) Bi = 10 (b) Bi = 10^4.

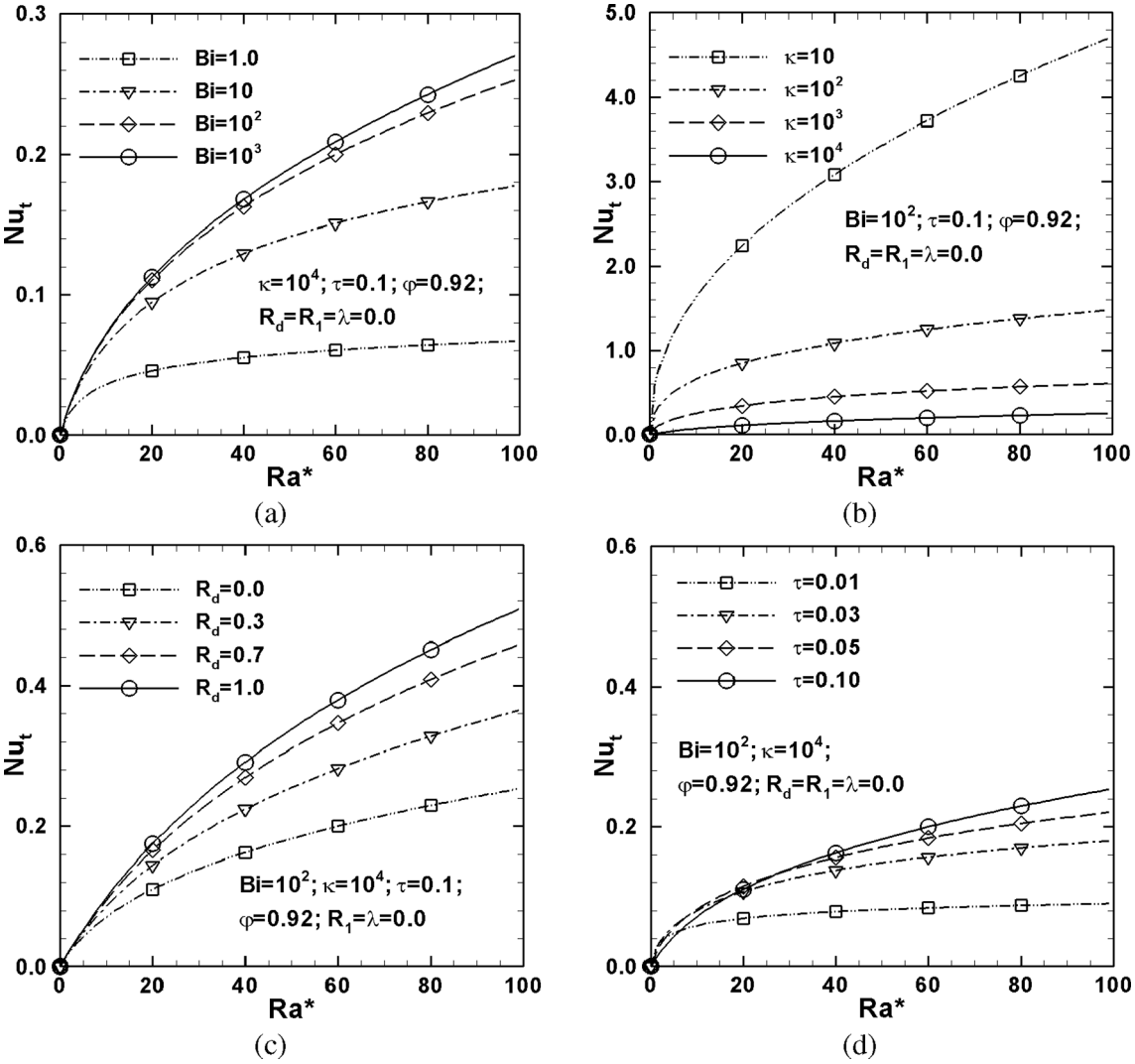

Fig. 15. Total Nusselt number of the porous fin as a function of di Ra* for: (a) Bi = 1.0 ÷ 10^3 (b) κ = 10 ÷ 10^3 (c) R_d = 10 ÷ 10^3 (d) τ = 0.01 ÷ 0.1.

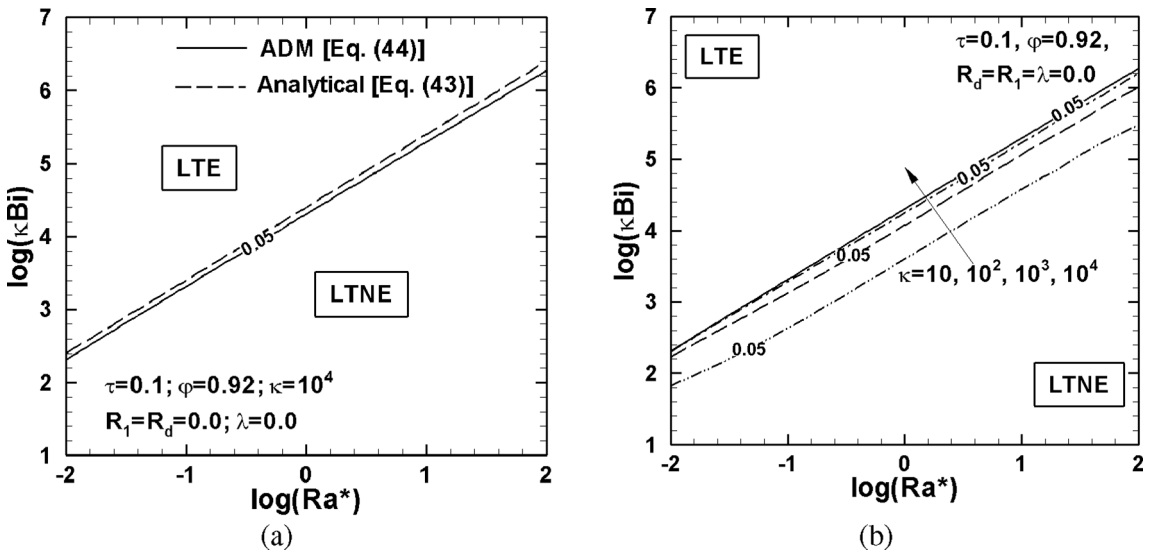

Fig. 16. Maps of LTE and LTNE: (a) comparison between scale analysis criteria, Eq. (43), and Adomian solution, Eq. (44), (b) effect of the conductive thermal ratio κ on the maps for LTE conditions.

anticipated, were observed for the lowest *Bi* value. The highest differences were detected close to the base of the fin. The effects of Ra^* for assigned *Bi* value were significant and the percentage differences, referred to the base temperature, at the tip of the fin between the solid and fluid temperature profiles were, for low $Bi = 1.0$, 52% and 3% for $Ra^*=10^3$ and 1.0, respectively. For $Bi = 100$ the values were 1% and practically zero for $Ra^*=10^3$ and 1.0, respectively. For assigned *Bi* value, the external convection increase determined lower differences between the solid phase and fluid phase temperature profiles.

The increase in thermal conductivity ratio provided a lower thermal resistance of the solid phase and a higher solid phase temperature for assigned *Bi* and Ra^* and an increase of differences between solid and fluid phase temperature profiles was observed.

The total Nusselt number increased as Ra^* and *Bi* increase, i.e., the heat transfer removed from the porous fin increased. Nu_t presented an asymptotic profile for $Bi = 10^4$ which corresponds to the local thermal equilibrium condition. The LTE assumption determines an overestimation of Nu_t with respect to the local thermal non-equilibrium (LTNE) assumption.

Criteria to compare local thermal non-equilibrium (LTNE) and local thermal equilibrium (LTE) assumptions were found with the solutions carried out by ADM and scale analysis and they were in good agreement. The criteria pointed out that for external convection and radiation parameters, the minimum Biot number decrease in order to assume more correctly the LTE, as the Rayleigh number and thermal conductivity ratio decrease.

CRediT authorship contribution statement

Bernardo Buonomo: Conceptualization, Methodology, Data curation, Writing - original draft, Writing - review & editing. **Furio Cascetta:** Methodology, Writing - review & editing. **Oronzio Manca:** Methodology, Writing - review & editing. **Mikhail Sheremet:** Methodology, Writing - review & editing.

Declaration of Competing Interest

The authors declare that they have no known competing financial interests or personal relationships that could have appeared to influence the work reported in this paper.

Acknowledgements

This research was partially funded by MIUR (Ministero dell'Istruzione, dell'Università e della Ricerca), grant number PRIN-2017F7KZWS and by Università degli Studi della Campania "Luigi Vanvitelli" with the grant number D.R. n. 138 under NanoTES project - V:ALERE program 2020.

The Authors would like to thank the Editor managing the review process and the Reviewers very much for their valuable suggestions and comments that have allowed to significantly improve the manuscript.

Appendix A

The Adomian polynomials for nonlinear function $N(\theta) = \theta^2$ are obtained as follows:

$$\left(\sum_{i=0}^{n}\lambda^i\theta_i\right)^2 = \left(\theta_0+\lambda\theta_1+\lambda^2\theta_2+....+\lambda^n\theta_n\right)\left(\sum_{i=0}^{n}\lambda^i\theta_i\right) = \left(\sum_{k=0}^{n}\theta_k\sum_{i=0}^{n}\lambda^{i+k}\theta_i\right) \tag{A1}$$

$$A_n = \frac{1}{n!}\left[\frac{d^n}{d\lambda^n}\left(\sum_{n=0}^{\infty}\lambda^n\theta_n\right)^2\right]_{\lambda=0} = \frac{1}{n!}\left[\frac{d^n}{d\lambda^n}\left(\sum_{k=0}^{n}\theta_k\sum_{i=0}^{n}\lambda^{i+k}\theta_i\right)\right]_{\lambda=0} = \\ = \frac{1}{n!}\sum_{k=0}^{n}\theta_k\left[\frac{d^n}{d\lambda^n}\sum_{i=0}^{n}\lambda^{i+k}\theta_i\right]_{\lambda=0} = \sum_{k=0}^{n}\theta_k\theta_{n-k} \tag{A2}$$

Appendix B

Eqs. (39) and (31) taking into account eq. (32) and inverse operator:
for $n = 1$

$$\theta_{1,s} = \alpha L_X^{-1}\theta_{0,s} - \beta L_X^{-1}\theta_{0,f} = (\alpha\theta_{0,s} - \beta\theta_{0,f})L_X^{-1}(1) = \frac{1}{2}(\alpha\theta_{0,s} - \beta\theta_{0,f})X^2 = \widetilde{\theta}_{1,s}X^2$$

$$\theta_{1,f} = \left(\delta\theta_{0,f} + \gamma\theta_{0,f}^2 - \delta\theta_{0,s}\right)L_X^{-1}(1) = \frac{1}{2}\left(\delta\theta_{0,f} + \gamma\theta_{0,f}^2 - \delta\theta_{0,s}\right)X^2 = \widetilde{\theta}_{1,f}X^2$$

with:

$$\widetilde{\theta}_{1,s} = \frac{1}{2}(\alpha\theta_{0,s} - \beta\theta_{0,f});\ \widetilde{\theta}_{1,f} = \frac{1}{2}\left(\delta\theta_{0,f} + \gamma\theta_{0,f}^2 - \delta\theta_{0,s}\right)$$

for $n = 2$

$$\theta_{2,s} = \alpha L_X^{-1}\theta_{1,s} - \beta L_X^{-1}\theta_{1,f} = \left(\alpha\widetilde{\theta}_{1,s} - \beta\widetilde{\theta}_{1,f}\right)L_X^{-1}(\xi^2) = \frac{1}{12}\left(\alpha\widetilde{\theta}_{1,s} - \beta\widetilde{\theta}_{1,f}\right)X^4 = \widetilde{\theta}_{2,s}X^4$$

$$\theta_{2,f} = \delta L_X^{-1}\theta_{1,f} + \gamma L_X^{-1}\sum_{k=0}^{1}\theta_{k,f}\theta_{1-k,f} - \delta L_X^{-1}\theta_{1,s} = \left[\delta\left(\widetilde{\theta}_{1,f} - \widetilde{\theta}_{1,s}\right) + \gamma\sum_{k=0}^{1}\widetilde{\theta}_{k,f}\widetilde{\theta}_{1-k,f}\right]L_X^{-1}(\xi^2) =$$

$$= \frac{1}{12}\left[\delta\left(\widetilde{\theta}_{1,f} - \widetilde{\theta}_{1,s}\right) + \gamma\sum_{k=0}^{1}\widetilde{\theta}_{k,f}\widetilde{\theta}_{1-k,f}\right]X^4 = \widetilde{\theta}_{2,f}X^4$$

with:

$$\widetilde{\theta}_{2,s} = \frac{1}{12}\left(\alpha\widetilde{\theta}_{1,s} - \beta\widetilde{\theta}_{1,f}\right);\ \widetilde{\theta}_{2,f} = \frac{1}{12}\left[\delta\left(\widetilde{\theta}_{1,f} - \widetilde{\theta}_{1,s}\right) + \gamma\sum_{k=0}^{1}\widetilde{\theta}_{k,f}\widetilde{\theta}_{1-k,f}\right]$$

for $n = 3$

$$\theta_{3,s} = \alpha L_X^{-1}\theta_{2,s} - \beta L_X^{-1}\theta_{2,f} = \left(\alpha\widetilde{\theta}_{2,s} - \beta\widetilde{\theta}_{2,f}\right)L_X^{-1}(\xi^4) = \frac{1}{30}\left(\alpha\widetilde{\theta}_{1,s} - \beta\widetilde{\theta}_{1,f}\right)X^6 = \widetilde{\theta}_{3,s}X^6$$

$$\theta_{3,f} = \delta L_X^{-1}\theta_{2,f} + \gamma L_X^{-1}\sum_{k=0}^{2}\theta_{k,f}\theta_{2-k,f} - \delta L_X^{-1}\theta_{2,s} = \left[\delta\left(\widetilde{\theta}_{2,f} - \widetilde{\theta}_{2,s}\right) + \gamma\sum_{k=0}^{2}\widetilde{\theta}_{k,f}\widetilde{\theta}_{2-k,f}\right]L_X^{-1}(\xi^4) =$$

$$= \frac{1}{30}\left[\delta\left(\widetilde{\theta}_{2,f} - \widetilde{\theta}_{2,s}\right) + \gamma\sum_{k=0}^{2}\widetilde{\theta}_{k,f}\widetilde{\theta}_{2-k,f}\right]X^6 = \widetilde{\theta}_{2,f}X^6$$

with:

$$\widetilde{\theta}_{3,s} = \frac{1}{30}\left(\alpha\widetilde{\theta}_{2,s} - \beta\widetilde{\theta}_{2,f}\right);\ \widetilde{\theta}_{2,f} = \frac{1}{30}\left[\delta\left(\widetilde{\theta}_{2,f} - \widetilde{\theta}_{2,s}\right) + \gamma\sum_{k=0}^{2}\widetilde{\theta}_{k,f}\widetilde{\theta}_{2-k,f}\right]$$

and for n-1 and n, according to the principle of mathematical induction, it results:

$$\theta_{n,s} = \alpha L_X^{-1}\theta_{n-1,s} - \beta L_X^{-1}\theta_{n-1,f} = \left(\alpha\widetilde{\theta}_{n-1,s} - \beta\widetilde{\theta}_{n-1,f}\right)L_X^{-1}\left(\xi^{2(n-1)}\right) =$$

$$= \frac{1}{2n(2n-1)}\left(\alpha\widetilde{\theta}_{n-1,s} - \beta\widetilde{\theta}_{n-1,f}\right)X^{2n} = \widetilde{\theta}_{n,s}X^{2n} \tag{B1}$$

$$\theta_{n,f} = \delta L_X^{-1}\theta_{n-1,f} + \gamma L_X^{-1}\sum_{k=0}^{n-1}\theta_{k,f}\theta_{n-1-k,f} - \delta L_X^{-1}\theta_{n-1,s} =$$

$$= \left[\delta\left(\widetilde{\theta}_{n-1,f} - \widetilde{\theta}_{n-1,s}\right) + \gamma\sum_{k=0}^{n-1}\widetilde{\theta}_{k,f}\widetilde{\theta}_{n-1-k,f}\right]L_X^{-1}\left(\xi^{2(n-1)}\right) = \tag{B2}$$

$$= \frac{1}{2n(2n-1)}\left[\delta\left(\widetilde{\theta}_{n-1,f} - \widetilde{\theta}_{n-1,s}\right) + \gamma\sum_{k=0}^{n-1}\widetilde{\theta}_{k,f}\widetilde{\theta}_{n-1-k,f}\right]X^6 = \widetilde{\theta}_{n-1,f}X^{2n}$$

$$\widetilde{\theta}_{n,s} = \frac{1}{2n(2n-1)}\left(\alpha\widetilde{\theta}_{n-1,s} - \beta\widetilde{\theta}_{n-1,f}\right);\ \widetilde{\theta}_{n,f} = \frac{1}{2n(2n-1)}\left[\delta\left(\widetilde{\theta}_{n-1,f} - \widetilde{\theta}_{n-1,s}\right) + \gamma\sum_{k=0}^{n-1}\widetilde{\theta}_{k,f}\widetilde{\theta}_{n-1-k,f}\right] \tag{B3}$$

References

[1] A.D. Kraus, A. Aziz, J. Welty, Extended surface heat transfer, John Wiley & Sons, New York, 2001.
[2] K. Vafai, Handbook of Porous Media, third ed., CRC Press, New York, 2015.
[3] D.A. Nield, A. Bejan, Convection in Porous Media, fifth ed., Springer, New York, 2017.
[4] H. Panchal, R. Sathyamurthi, Experimental analysis of single-basin solar still with porous fins, Int. J. Ambient Energy 41 (5) (2020) 563–569, https://doi.org/10.1080/01430750.2017.1360206.
[5] F. Selimefendigil, F. Bayrak, H.F. Oztop, Experimental analysis and dynamic modeling of a photovoltaic module with porous fins, Renew. Energy 125 (2018) 193–205, https://doi.org/10.1016/j.renene.2018.02.002.
[6] S.-L. Wang, X.-Y. Li, X.-D. Wang, G. Lu, Flow and heat transfer characteristics in double-layered microchannel heat sinks with porous fins, Int. Commun. Heat Mass Transfer 93 (2018) 41–47, https://doi.org/10.1016/j.icheatmasstransfer.2018.03.003.
[7] G.A. Oguntala, G.M. Sobamowo, R.A. Abd-Alhameed, J.M. Noras, Numerical Study of Performance of Porous Fin Heat Sink of Functionally Graded Material for Improved Thermal Management of Consumer Electronics IEEE Transactions on Components, Packaging and Manufacturing Technology 9 (7) (2019) art. no. 8675472, pp. 1271-1283. DOI: 10.1109/TCPMT.2019.2907150.
[8] S. Kiwan, H. Alwan, N. Abdelal, An experimental investigation of the natural convection heat transfer from a vertical cylinder using porous fins, Appl. Therm. Eng. 179 (2020) art. no. 115673. DOI: 10.1016/j.applthermaleng.2020.115673.
[9] T. Deshamukhya, D. Bhanja, S. Nath, Heat transfer enhancement through porous fins: A comprehensive review of recent developments and innovations, Proceedings of the Institution of Mechanical Engineers, Part C: J. Mech. Eng. Sci. 235 (5) (2021) 946–960, https://doi.org/10.1177/0954406220939600.
[10] S. Kiwan, M. Al-Nimr, Using porous fins for heat transfer enhancement, ASME J. Heat Transfer 123 (2001) 790–795, https://doi.org/10.1115/1.1371922.
[11] S. Kiwan, Thermal analysis of natural convection porous fins, Transp. Porous Media 67 (1) (2007) 17–29, https://doi.org/10.1007/s11242-006-0010-3.
[12] S. Kiwan, Effect of radiative losses on the heat transfer from porous fins, Int. J. Therm. Sci. 46 (10) (2007) 1046–1055, https://doi.org/10.1016/j.ijthermalsci.2006.11.013.
[13] A.R.A. Khaled, Investigation of heat transfer enhancement through permeable fins, J. Heat Transfer 132 (3) (2010) 1–5, https://doi.org/10.1115/1.4000056.
[14] M. Hamdan, M.A. Al-Nimr, The Use of Porous Fins for Heat Transfer Augmentation in Parallel-Plate Channels, Transp. Porous Media 84 (2) (2010) 409–420, https://doi.org/10.1007/s11242-009-9510-2.
[15] R.S.R. Gorla, A.Y. Bakier, Thermal analysis of natural convection and radiation in porous fins, Int. Commun. Heat Mass Transfer 38 (5) (2011) 638–645, https://doi.org/10.1016/j.icheatmasstransfer.2010.12.024.
[16] B. Kundu, D. Bhanja, An analytical prediction for performance and optimum design analysis of porous fins, Int. J. Refrig 34 (1) (2011) 337–352, https://doi.org/10.1016/j.ijrefrig.2010.06.011.
[17] D. Bhanja, B. Kundu, Thermal analysis of a constructal T-shaped porous fin with radiation effects, Int. J. Refrig 34 (6) (2011) 1483–1496, https://doi.org/10.1016/j.ijrefrig.2011.04.003.
[18] I. Rahimi Petroudi, D.D. Ganji, A.B. Shotorban, M.K. Nejad, E. R. Rahimi Rohollahtabar, F. Taherinia, Semi-analytical method for solving non-linear equation arising of natural convection porous fin, Therm. Sci. 16(5) (2012) 1303–1308. doi: 10.2298/TSCI1205303P.
[19] B. Kundu, D. Bhanja, K.-S. Lee, A model on the basis of analytics for computing maximum heat transfer in porous fins, Int. J. Heat Mass Transf. 55 (25–26) (2012) 7611–7622, https://doi.org/10.1016/j.ijheatmasstransfer.2012.07.069.
[20] M. Torabi, H. Yaghoobi, Series solution for convective-radiative porous fin using differential transformation method, J. Porous Media 16 (4) (2013) 341–349, https://doi.org/10.1615/JPorMedia.v16.i4.
[21] M.T. Darvishi, R.S.R. Gorla, F. Khani, Natural convection and radiation in porous fins, Int. J. Numer. Meth. Heat Fluid Flow 23 (2013) 1406–1430, https://doi.org/10.1108/HFF-12-2011-0264.
[22] S. Saedodin, M. Shahbabaei, Thermal Analysis of Natural Convection in Porous Fins with Homotopy Perturbation Method (HPM), Arabian J. Sci. Eng. 38 (8) (2013) 2227–2231, https://doi.org/10.1007/s13369-013-0581-6.
[23] D. Bhanja, B. Kundu, P.K. Mandal, Thermal analysis of porous pin fin used for electronic cooling, Procedia Eng. 64 (2013) 956–965, https://doi.org/10.1016/j.proeng.2013.09.172.
[24] S. Saedodin, S. Sadeghi, Temperature distribution in long porous fins in natural convection condition, Middle East J. Sci. Res. 13 (6) (2013) 812–817, https://doi.org/10.5829/idosi.mejsr.2013.13.6.2436.
[25] M. Hatami, A. Hasanpour, D.D. Ganji, Heat transfer study through porous fins (Si3N4 and AL) with temperature-dependent heat generation, Energy Convers. Manage. 74 (2013) 9–16, https://doi.org/10.1016/j.enconman.2013.04.034.
[26] M. Hatami, D.D. Ganji, Thermal performance of circular convective-radiative porous fins with different section shapes and materials, Energy Convers. Manage. 76 (2013) 185–193, https://doi.org/10.1016/j.enconman.2013.07.040.
[27] A. Moradi, A.P.M. Fallah, T. Hayat, O.M. Aldossary, On Solution of Natural Convection and Radiation Heat Transfer Problem in a Moving Porous Fin, Arabian J. Sci. Eng. 39 (2) (2014) 1303–1312, https://doi.org/10.1007/s13369-013-0708-9.
[28] A. Moradi, T. Hayat, A. Alsaedi, Convection-radiation thermal analysis of triangular porous fins with temperature-dependent thermal conductivity by DTM, Energy Convers. Manage. 77 (2014) 70–77, https://doi.org/10.1016/j.enconman.2013.09.016.
[29] M. Hatami, D.D. Ganji, Investigation of refrigeration efficiency for fully wet circular porous fins with variable sections by combined heat and mass transfer analysis, Int. J. Refrig 40 (2014) 140–151, https://doi.org/10.1016/j.ijrefrig.2013.11.002.
[30] M. Hatami, D.D. Ganji, Thermal behavior of longitudinal convective-radiative porous fins with different section shapes and ceramic materials (SiC and Si3N 4), Ceram. Int. 40 (5) (2014) 6765–6775, https://doi.org/10.1016/j.ceramint.2013.11.140.
[31] M. Turkyilmazoglu, Efficiency of heat and mass transfer in fully wet porous fins: Exponential fins versus straight fins, Int. J. Refrig 46 (2014) 158–164, https://doi.org/10.1016/j.ijrefrig.2014.04.011.
[32] R. Das, Forward and inverse solutions of a conductive, convective and radiative cylindrical porous fin, Energy Convers. Manage. 87 (2014) 96–106, https://doi.org/10.1016/j.enconman.2014.06.096.
[33] B. Kundu, K.-S. Lee, Exact analysis for minimum shape of porous fins under convection and radiation heat exchange with surrounding, Int. J. Heat Mass Transf. 81 (2015) 439–448, https://doi.org/10.1016/j.ijheatmasstransfer.2014.10.044.
[34] M. Shahbabaei, D.D. Ganji, Prediction of a semi-exact analytic solution of a convective porous fin with variable cross section by different methods, Walailak J. Sci. Technol. 12 (10) (2015) 909–921.
[35] A. Vahabzadeh, D.D. Ganji, M. Abbasi, Analytical investigation of porous pin fins with variable section in fully wet conditions, Case Studies Therm. Eng. 5 (2015) 1–12, https://doi.org/10.1016/j.csite.2014.11.002.
[36] M.T. Darvishi, R.S.R. Gorla, F. Khani, A. Aziz, Thermal performance of a porous radial fin with natural convection and radiative heat losses, Therm. Sci. 9 (2) (2015) 669–678, https://doi.org/10.2298/TSCI120619149D.
[37] E. Cuce, P.M. Cuce, A successful application of homotopy perturbation method for efficiency and effectiveness assessment of longitudinal porous fins, Energy Convers. Manage. 93 (2015) 92–99, https://doi.org/10.1016/j.enconman.2015.01.003.
[38] T. Patel, R. Meher, A Study on Temperature Distribution, Efficiency and Effectiveness of Longitudinal Porous Fins by Using Adomian Decomposition Sumudu Transform Method, Procedia Eng. 127 (2015) 751–758, https://doi.org/10.1016/j.proeng.2015.11.409.
[39] M.T. Darvishi, R.S.R. Gorla, F. Khani, B.J. Gireesha, Thermal analysis of natural convection and radiation in a fully wet porous fin, Int. J. Numer. Meth. Heat Fluid Flow 26 (8) (2016) 2419–2431, https://doi.org/10.1108/HFF-06-2015-0230.
[40] B. Kundu, K.-S. Lee, A proper analytical analysis of annular step porous fins for determining maximum heat transfer, Energy Convers. Manage. 110 (2016) 469–480, https://doi.org/10.1016/j.enconman.2015.09.037.
[41] K. Singh, R. Das, B. Kundu, Approximate analytical method for porous stepped fins with temperature-dependent heat transfer parameters, J. Thermophys. Heat Transfer 30 (3) (2016) 661–672, https://doi.org/10.2514/1.T4831.
[42] J. Ma, Y. Sun, B. Li, H. Chen, Spectral collocation method for radiative–conductive porous fin with temperature dependent properties, Energy Convers. Manage. 111 (2016) 279–288, https://doi.org/10.1016/j.enconman.2015.12.054.
[43] F. Khani, M.T. Darvishi, R.S.R. Gorla, B.J. Gireesha, Thermal analysis of a fully wet porous radial fin with natural convection and radiation using the spectral collocation method, Int. J. Appl. Mech. Eng. 21 (2) (2016) 377–392, https://doi.org/10.1515/ijame-2016-0023.
[44] T.G. Motsumi, Investigation of heat transfer enhancement through porous radial fins with variable thermal conductivity, JP J. Heat Mass Transf. 13 (2) (2016) 239–252, https://doi.org/10.17654/HM013020239.
[45] S.A. Hazarika, T. Deshamukhya, D. Bhanja, S. Nath, Thermal analysis of a constructal T-shaped porous fin with simultaneous heat and mass transfer, Chin. J. Chem. Eng. 25 (9) (2017) 1121–1136, https://doi.org/10.1016/j.cjche.2017.03.034.
[46] J. Ma, Y. Sun, B. Li, Simulation of combined conductive, convective and radiative heat transfer in moving irregular porous fins by spectral element method, Int. J. Therm. Sci. 118 (2017) 475–487, https://doi.org/10.1016/j.ijthermalsci.2017.05.008.
[47] H. Asadian, M. Zaretabar, D.D. Ganji, M. Gorji-Bandpy, S. Sohrabi, Investigation of Heat Transfer in Rectangular Porous Fins (Si 3 N 4) with Temperature-Dependent Internal Heat Generation by Galerkin's Method (GM) and Akbari-

Ganji's Method (AGM), Int. J. Appl. Comput. Math. 3 (4) (2017) 2987–3000, https://doi.org/10.1007/s40819-016-0279-z.
[48] M.G. Sobamowo, O.M. Kamiyo, O.A. Adeleye, Thermal performance analysis of a natural convection porous fin with temperature-dependent thermal conductivity and internal heat generation, Therm. Sci. Eng. Prog. 1 (2017) 39–52, https://doi.org/10.1016/j.tsep.2017.02.007.
[49] T. Deshamukhya, D. Bhanja, S. Nath, A. Maji, G. Choubey, Analytical study of temperature distribution in a rectangular porous fin considering both insulated and convective tip, AIP Conference Proceedings 1859 (2017) art. no. 020031. doi: 10.1063/1.4990184.
[50] A.R. Shateri, B. Salahshour, Comprehensive thermal performance of convection–radiation longitudinal porous fins with various profiles and multiple nonlinearities, Int. J. Mech. Sci. 136 (2018) 252–263, https://doi.org/10.1016/j.ijmecsci.2017.12.030.
[51] H.A. Hoshyar, I. Rahimipetroudi, D.D. Ganji, Heat Transfer Performance on Longitudinal Porous Fins with Temperature-Dependent Heat Generation, Heat Transfer Coefficient and Surface Emissivity, Iranian J. Sci. Technol. Trans. Mech. Eng. 43 (2) (2019) 383–391, https://doi.org/10.1007/s40997-017-0126-9.
[52] O. Zargar, M. Mollaghaee-Roozbahani, M. Bashirpour, M. Baghani, The Application of Homotopy Analysis Method to Determine the Thermal Response of Convective-Radiative Porous Fins with Temperature-Dependent Properties, International Journal of Applied Mechanics 11 (9) (2019) art. no. 1950089. doi: 10.1142/S1758825119500893.
[53] S. Hoseinzadeh, P.S. Heyns, A.J. Chamkha, A. Shirkhani, Thermal analysis of porous fins enclosure with the comparison of analytical and numerical methods, J. Therm. Anal. Calorim. 138 (1) (2019) 727–735, https://doi.org/10.1007/s10973-019-08203-x.
[54] S. Kiwan, On the Natural Convection Heat Transfer from an Inclined Surface with Porous Fins, Transp. Porous Media 127 (2) (2019) 295–307, https://doi.org/10.1007/s11242-018-1192-1.
[55] S. Hoseinzadeh, A. Moafi, A. Shirkhani, A.J. Chamkha, Numerical validation heat transfer of rectangular cross-section porous fins, J. Thermophys Heat Transfer 33 (3) (2019) 698–704, https://doi.org/10.2514/1.T5583.
[56] S. Abbasbandy, E. Shivanian, The exact closed solution in the analysis of a natural convection porous fin with temperature-dependent thermal conductivity and internal heat generation, Can. J. Phys. 97 (5) (2019) 566–575, https://doi.org/10.1139/cjp-2018-0242.
[57] B.J. Gireesha, G. Sowmya, M. Macha, Temperature distribution analysis in a fully wet moving radial porous fin by finite element method, International Journal of Numerical Methods for Heat and Fluid Flow (2019) in press. doi: 10.1108/HFF-12-2018-0744.
[58] P.L. Ndlovu, R.J. Moitsheki, Thermal analysis of natural convection and radiation heat transfer in moving porous fins, Frontiers in Heat and Mass Transfer 12 (2019) art. no. 7. doi: 10.5098/hmt.12.7.
[59] F. Shafiei, M.R. Talaghat, Numerical and Galerkin's methods for thermal performance analysis of circular porous fins with various profiles when the surface temperature is higher/lower than the air temperature, Energy Sources, Part A: Recovery, Utilization and Environmental Effects in press (2019). doi: 10.1080/15567036.2019.1677816.
[60] P.L. Ndlovu, R.J. Moitsheki, Steady state heat transfer analysis in a rectangular moving porous fin, Propul. Power Res. 9 (2) (2020) 188–196, https://doi.org/10.1016/j.jppr.2020.03.002.
[61] G. Sowmya, B.J. Gireesha, O.D. Makinde, Thermal performance of fully wet longitudinal porous fin with temperature-dependent thermal conductivity, surface emissivity and heat transfer coefficient, Multidiscipline Modeling Mater. Struct. 16 (4) (2020) 749–764, https://doi.org/10.1108/MMMS-08-2019-0147.
[62] A. Gupta, Gautam, S. Sahoo, A. Mohanty, Performance evaluation of porous fin with prescribed tip temperature: An analytical and numerical approach, Int. J. Heat Mass Transf. 156 (2020) 119736, https://doi.org/10.1016/j.ijheatmasstransfer.2020.119736.
[63] G. Sowmya, M.I. Khan, S. Momani, T. Hayat, Thermal investigation of fully wet longitudinal porous fin of functionally graded material, Int. J. Numer. Methods Heat Fluid Flow 30 (12) (2020) 5087–5101, https://doi.org/10.1108/HFF-12-2019-0908.
[64] B.J. Gireesha, G. Sowmya, Heat transfer analysis of an inclined porous fin using Differential Transform Method, International Journal of Ambient Energy in press (2020). doi: 10.1080/01430750.2020.1818619.
[65] R. Das, B. Kundu, Prediction of heat generation in a porous fin from surface temperature, J. Thermophys Heat Transfer 31 (4) (2017) 781–790, https://doi.org/10.2514/1.T5098.
[66] M. Baghban, Z. Shams, A. Ebrahimifakhar, Inverse analysis of a porous fin to estimate time-dependent base temperature, J. Thermophys Heat Transfer 32 (1) (2018) 27–34, https://doi.org/10.2514/1.T5004.
[67] S.-H. Park, T.H. Kim, J.H. Jeong, Experimental investigation of the convective heat transfer coefficient for open-cell porous metal fins at low Reynolds numbers, Int. J. Heat Mass Transf. 100 (2016) 608–614, https://doi.org/10.1016/j.ijheatmasstransfer.2016.04.114.
[68] G. Sowmya, B.J. Gireesha, B.C. Prasannakumara, Scrutinization of different shaped nanoparticle of molybdenum disulfide suspended nanofluid flow over a radial porous fin, Int. J. Numer. Meth. Heat Fluid Flow 30 (7) (2019) 3685–3699, https://doi.org/10.1108/HFF-08-2019-0622.
[69] B.J. Gireesha, G. Sowmya, M.I. Khan, H.F. Öztop, Flow of hybrid nanofluid across a permeable longitudinal moving fin along with thermal radiation and natural convection, Comput. Methods Programs Biomed. 185 (2020) 105166, https://doi.org/10.1016/j.cmpb.2019.105166.
[70] B.J. Gireesha, G. Sowmya, R.S.R. Gorla, Nanoparticle shape effect on the thermal behaviour of moving longitudinal porous fin, Proceedings of the Institution of Mechanical Engineers, Part N: Journal of Nanomaterials, Nanoengineering and Nanosystems 234 (3–4) (2020) 115–121. doi: 10.1177/2397791420915139.
[71] A. Baslem, G. Sowmya, B.J. Gireesha, B.C. Prasannakumara, M. Rahimi-Gorji, N. M. Hoang, Analysis of thermal behavior of a porous fin fully wetted with nanofluids: convection and radiation, J. Mol. Liquids 307 (2020) 112920, https://doi.org/10.1016/j.molliq.2020.112920.
[72] G. Sowmya, B.J. Gireesha, S. Sindhu, B.C. Prasannakumara, Investigation of Ti6Al4V and AA7075 alloy embedded nanofluid flow over longitudinal porous fin in the presence of internal heat generation and convective condition, Commun. Theoret. Phys. 72 (2) (2020), 025004, https://doi.org/10.1088/1572-9494/ab6904.
[73] R. Das, K.T. Ooi, Predicting multiple combination of parameters for designing a porous fin subjected to a given temperature requirement, Energy Convers. Manage. 66 (2013) 211–219, https://doi.org/10.1016/j.enconman.2012.10.019.
[74] T. Deshamukhya, S.A. Hazarika, D. Bhanja, S. Nath, An optimization study to investigate non-linearity in thermal behaviour of porous fin having temperature dependent internal heat generation with and without tip loss, Commun. Nonlinear Sci. Numer. Simul. 67 (2019) 351–365, https://doi.org/10.1016/j.cnsns.2018.07.024.
[75] T. Deshamukhya, R. Nath, S.A. Hazarika, D. Bhanja, S. Nath, A modified firefly algorithm to maximize heat dissipation of a rectangular porous fin in heat exchangers exposed to both convective and radiative environment, Proceedings of the Institution of Mechanical Engineers, Part E: Journal of Process Mechanical Engineering 233 (6) (2019) 1203–1216, https://doi.org/10.1177/0954408919861244.
[76] I. Ahmad, H. Zahid, F. Ahmad, M.A.Z. Raja, D. Baleanu, Design of computational intelligent procedure for thermal analysis of porous fin model, Chin. J. Phys. 59 (2019) 641–655, https://doi.org/10.1016/j.cjph.2019.04.015.
[77] G. Oguntala, G. Sobamowo, R. Abd-Alhameed, Numerical investigation of inclination on the thermal performance of porous fin heat sink using pseudospectral collocation method, Karbala Int. J. Modern Sci. 5 (1) (2019) 4, https://doi.org/10.33640/2405-609X.1013.
[78] T. Deshamukhya, D. Bhanja, S. Nath, Application of metaheuristic algorithms in optimum thermal design analysis of a rectangular porous fin subjected to both insulated and convective tip conditions, Proceedings of the Institution of Mechanical Engineers, Part A: Journal of Power and Energy 234 (8) (2020) 1175–1188, https://doi.org/10.1177/0957650919899559.
[79] W. Waseem, M. Sulaiman, S. Islam, P. Kumam, R. Nawaz, M.A.Z. Raja, M. Farooq, M. Shoaib, A study of changes in temperature profile of porous fin model using cuckoo search algorithm, Alexandria Eng. J. 59 (1) (2020) 11–24, https://doi.org/10.1016/j.aej.2019.12.001.
[80] A. Taklifi, C. Aghanajafi, H. Akrami, The Effect of MHD on a porous fin attached to a vertical isothermal surface, Transp. Porous Media 85 (1) (2010) 215–231, https://doi.org/10.1007/s11242-010-9556-1.
[81] H.A. Hoshyar, D.D. Ganji, A. Majidian, Least square method for porous fin in the presence of uniform magnetic field, J. Appl. Fluid Mech. 9 (2) (2016) 661–668, https://doi.org/10.18869/acadpub.jafm.68.225.24245.
[82] T. Patel, R. Meher, Thermal analysis of porous fin with uniform magnetic field using Adomian decomposition Sumudu transform method, Nonlinear Eng. 6 (3) (2017) 191–200, https://doi.org/10.1515/nleng-2017-0021.
[83] G. Oguntala, R. Abd-Alhameed, M. Ngala, Transient thermal analysis and optimization of convective-radiative porous fin under the influence of magnetic field for efficient microprocessor cooling, Int. J. Therm. Sci. 145 (2019) 106019, https://doi.org/10.1016/j.ijthermalsci.2019.106019.
[84] G. Oguntala, G. Sobamowo, R. Abd-Alhameed, S. Jones, Efficient iterative method for investigation of convective–radiative porous fin with internal heat generation under a uniform magnetic field, Int. J. Appl. Comput. Math. 5 (1) (2019) 13, https://doi.org/10.1007/s40819-018-0592-9.
[85] M. Nabati, M. Jalalvand, S. Taherifar, Sinc collocation approach through thermal analysis of porous fin with magnetic field, J. Therm. Anal. Calorim. 144 (6) (2021) 2145–2158, https://doi.org/10.1007/s10973-020-09923-1.
[86] P.L. Ndlovu, Analytical study of transient heat transfer in a triangular moving porous fin with temperature dependent thermal properties, Defect Diffusion Forum 393 (2019) 31–46, https://doi.org/10.4028/www.scientific.net/DDF.393.31.
[87] P.L. Ndlovu, Numerical analysis of transient heat transfer in radial porous moving fin with temperature dependent thermal properties, J. Appl. Comput. Mech. 6 (1) (2020) 137–144, https://doi.org/10.22055/jacm.2019.29271.1578.
[88] M. Mehraban, M.R. Khosravi-Nikou, F. Shaahmadi, Thermal behaviour of convective-radiative porous fins under periodic thermal conditions, Can. J. Chem. Eng. 97 (3) (2019) 821–828, https://doi.org/10.1002/cjce:v97.310.1002/cjce:23240.
[89] N. Targui, H. Kahalerras, Analysis of fluid flow and heat transfer in a double pipe heat exchanger with porous structures, Energy Convers. Manage. 49 (11) (2008) 3217–3229, https://doi.org/10.1016/j.enconman.2008.02.010.
[90] S. Kiwan, O. Zeitoun, Natural convection in a horizontal cylindrical annulus using porous fins, Int. J. Numer. Meth. Heat Fluid Flow 18 (5) (2008) 618–634, https://doi.org/10.1108/09615530810879747.
[91] Y.-T. Yang, K.-T. Tsai, H.-W. Tang, S.-E. Chung, Numerical simulations and optimization of porous pin fins in a rectangular channel, Numer. Heat Transf. Part A Appl. 70 (7) (2016) 791–808, https://doi.org/10.1080/10407782.2016.1214479.

[92] K. Bilen, S. Gok, A.B. Olcay, I. Solmus, Investigation of the effect of aluminum porous fins on heat transfer, Energy 138 (2017) 1187–1198, https://doi.org/10.1016/j.energy.2017.08.015.
[93] M. Mesgarpour, A. Heydari, S. Saddodin, Investigating the effect of connection type of a sintered porous fin through a channel on heat transfer and fluid flow, J. Therm. Anal. Calorim. 135 (1) (2019) 461–474, https://doi.org/10.1007/s10973-018-7356-y.
[94] K. Logesh, R. Arunraj, S. Govindan, M. Thangaraj, G.K. Yuvashree, Numerical investigation on possibility of heat transfer enchancement using reduced weight fin configuration, Int. J. Ambient Energy 41 (2) (2020) 142–145, https://doi.org/10.1080/01430750.2018.1451382.
[95] P.K. Srivastava, S.K. Agrawal, Winter and summer performance of single sloped basin type solar still integrated with extended porous fins, Desalination 319 (2013) 73–78, https://doi.org/10.1016/j.desal.2013.03.030.
[96] B. Alshuraiaan, K. Khanafer, The effect of the position of the heated thin porous fin on the laminar natural convection heat transfer in a differentially heated cavity, Int. Commun. Heat Mass Transf. 78 (2016) 190–199, https://doi.org/10.1016/j.icheatmasstransfer.2016.09.014.
[97] H. Zargartalebi, M. Ghalambaz, A. Noghrehabadi, A.J. Chamkha, Natural convection of a nanofluid in an enclosure with an inclined local thermal non-equilibrium porous fin considering Buongiorno's model, Numer. Heat Transf. Part A: Appl. 70 (4) (2016) 432–445, https://doi.org/10.1080/10407782.2016.1173483.
[98] M. Siavashi, R. Yousofvand, S. Rezanejad, Nanofluid and porous fins effect on natural convection and entropy generation of flow inside a cavity, Adv. Powder Technol. 29 (1) (2018) 142–156, https://doi.org/10.1016/j.apt.2017.10.021.
[99] A. Ghahremannezhad, K. Vafai, Thermal and hydraulic performance enhancement of microchannel heat sinks utilizing porous substrates, Int. J. Heat Mass Transf. 122 (2018) 1313–1326, https://doi.org/10.1016/j.ijheatmasstransfer.2018.02.024.
[100] G.A. Oguntala, R.A. Abd-Alhameed, G.M. Sobamowo, N. Eya, Effects of particles deposition on thermal performance of a convective-radiative heat sink porous fin of an electronic component, Therm. Sci. Eng. Prog. 6 (2018) 177–185, https://doi.org/10.1016/j.tsep.2017.10.019.
[101] G. Oguntala, R. Abd-Alhameed, Performance of convective-radiative porous fin heat sink under the influence of particle deposition and adhesion for thermal enhancement of electronic components, Karbala Int. J. Mod. Sci. 4 (3) (2018) 297–312, https://doi.org/10.1016/j.kijoms.2018.06.002.
[102] K. Vafai, M. Sozen, Analysis of energy and momentum transport for fluid flow through a porous bed, J. Heat Transfer 112 (1990) 690–699, https://doi.org/10.1115/1.2910442.
[103] M. Quintard, S. Whitaker, One and two equation models for transient diffusion processes in twophase systems, Adv. Heat Transfer 23 (1993) 369–465.
[104] A. Amiri, K. Vafai, Analysis of dispersion effects and non-thermal equilibrium, non-Darcian, variable porosity incompressible flow through porous media, Int. J. Heat Mass Transf. 37 (6) (1994) 939–954, https://doi.org/10.1016/0017-9310(94)90219-4.
[105] A.V. Kuznetsov, Thermal nonequilibrium forced convection in porous media, in: D.B. Ingham, I. Pop (Eds.), Transport Phenomena in Porous Media, Pergamon, Oxford, UK, 1998, pp. 103–129.
[106] W.J. Minkowycz, A. Haji-Sheikh, K. Vafai, On departure from local thermal equilibrium in porous media due to a rapidly changing heat source: the Sparrow number, Int. J. Heat Mass Transf. 42 (18) (1999) 3373–3385, https://doi.org/10.1016/S0017-9310(99)00043-5.
[107] P. Vadasz, On the paradox of heat conduction in porous media subject to lack of local thermal equilibrium, Int. J. Heat Mass Transf. 50 (21–22) (2007) 4131–4140, https://doi.org/10.1016/j.ijheatmasstransfer.2007.03.017.
[108] A. Barletta, D.A.S. Rees, Local thermal non-equilibrium effects in the Darcy-Bénard instability with isoflux boundary conditions, Int. J. Heat Mass Transf. 55 (1–3) (2012) 384–394, https://doi.org/10.1016/j.ijheatmasstransfer.2011.09.031.
[109] P. Vadasz, Small Nield number convection in a porous layer heated from below via a constant heat flux and subject to lack of local thermal equilibrium, J. Porous Media 15 (3) (2012) 249–258, https://doi.org/10.1615/JPorMedia.v15.i310.1615/JPorMedia.v15.i3.40.
[110] B. Straughan, Convection with Local Thermal Non-Equilibrium and Microfluidic Effects, Springer, Berlin/Heidelberg, Germany, 2015.
[111] B. Pulvirenti, M. Celli, A. Barletta, Flow and Convection in Metal Foams: A Survey and New CFD Results, Fluids 5 (3) (2020) 155, https://doi.org/10.3390/fluids5030155.
[112] M. Kaviany, Principles of Heat Transfer in Porous Media, 2nd ed., Springer Verlag, New York, 1995.
[113] G. Adomian, A review of the decomposition method in applied mathematics, J. Math. Anal. Appl. 135 (2) (1988) 501–544, https://doi.org/10.1016/0022-247X(88)90170-9.
[114] G. Adomian, Solving Frontier Problems of Physics: The Decomposition Method, Kluwer Academic Publishers, 1994.
[115] T.J. Ypma, Historical development of the Newton-Raphson method, SIAM Rev. 37 (4) (1995) 531–551, https://doi.org/10.1137/1037125.
[116] D. Bhanja, B. Kundu, A. Aziz, Enhancement of heat transfer from a continuously moving porous fin exposed in convective–radiative environment, Energy Convers. Manage. 88 (2014) 842–853, https://doi.org/10.1016/j.enconman.2014.09.016.
[117] S.J. Kim, S.P. Jang, Effects of the Darcy number, the Prandtl number, and the Reynolds number on local thermal non-equilibrium, Int. J. Heat Mass Transf. 45 (19) (2002) 3885–3896, https://doi.org/10.1016/S0017-9310(02)00109-6.